

Amplification of vacuum fluctuations and the dynamical Casimir effect in superconducting circuits

Robert Johansson
iTHES Research Group, RIKEN

Collaborators:

F. Nori
(RIKEN)

G. Johansson, C. Wilson, P. Delsing,
A. Pourkabirian, M. Simoen, T. Duty
(Chalmers)

P. Nation and M. Blencowe
(Korea University, Dartmouth)

Theory:

Phys. Rev. Lett. 103, 147003 (2009)

Phys. Rev. A 82, 052509 (2010)

Phys. Rev. A 87, 043804 (2013)

Experiment:

Nature 479, 376 (2011)

Review:

Rev. Mod. Phys. 84, 1 (2012)

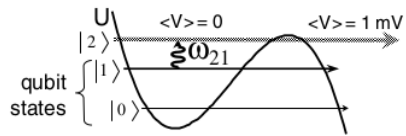
Content

- Quantum optics in superconducting circuits
- Overview of quantum vacuum effects
- Dynamical Casimir effect in superconducting circuits
- Review of experimental results
- Summary

Overview of superconducting circuits

from qubits to on-chip quantum optics

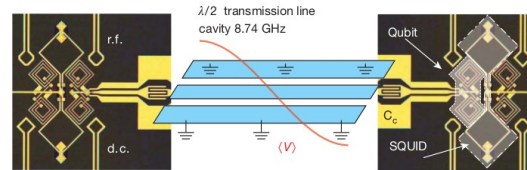
qubits



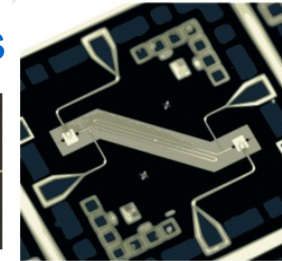
NIST 2002

qubit-qubit

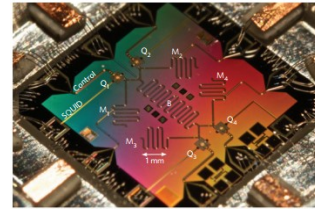
resonator as coupling bus



NIST 2007



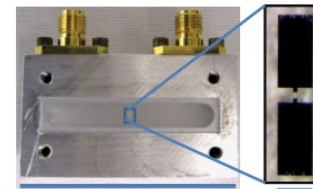
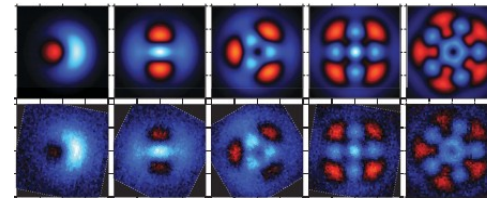
UCSB 2009



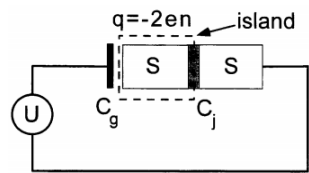
UCSB 2012

high level of control of resonators

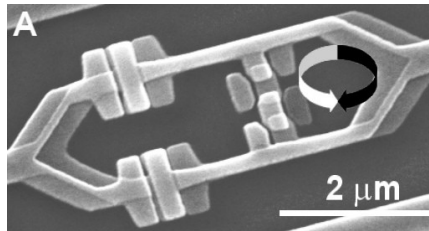
UCSB 2009



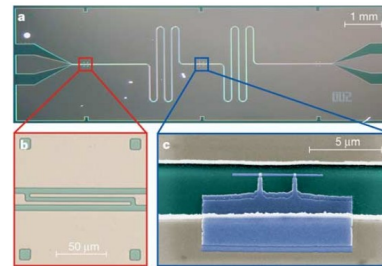
Yale 2011



Saclay 1998



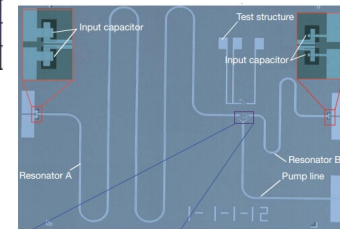
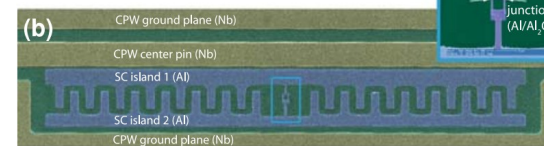
Delft 2003



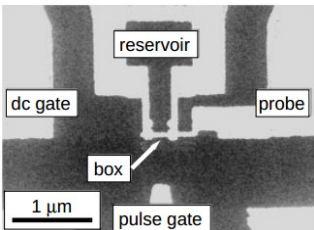
Yale 2004

qubit-resonator

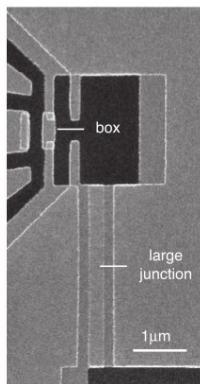
Yale 2008



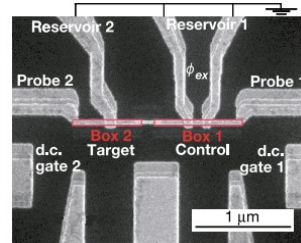
ETH 2010



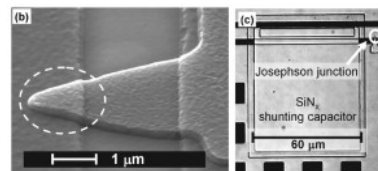
NEC 1999



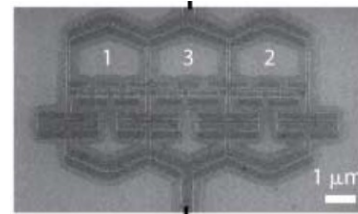
Saclay 2002



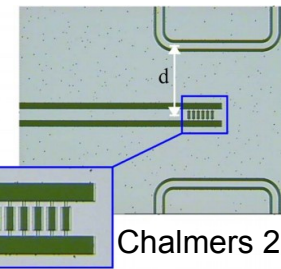
NEC 2003



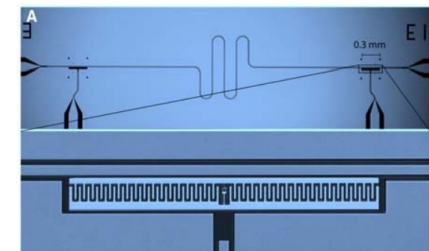
UCSB 2006



NEC 2007



Chalmers 2008



ETH 2008

2000

2005

2010

3

Comparison: Quantum optics and μw circuits

Similarities

Essentially the same physics

Electromagnetic fields, quantum mechanics, all essentially the same... but there are some practical differences:

Differences

Frequency / Temperature

Microwave fields have orders of magnitudes lower frequencies than optical fields. Optics experiment can be at room temperature or at least much higher temperature than microwave circuits, which has to be at cryogenic temperatures due to the lower frequency

Controllability / Dissipation

Microwave circuits can be designed and controlled more easily, which is sometimes an advantage, but is also closely related to shorter coherence times

Interaction strengths

Microwave circuits are much larger, and can have larger dipole moments and therefore interaction strengths

Measurement capabilities

Single-photon detection not readily available for microwave fields, but measuring the field quadratures with linear amplifier is easier than in microwave fields than in quantum optics

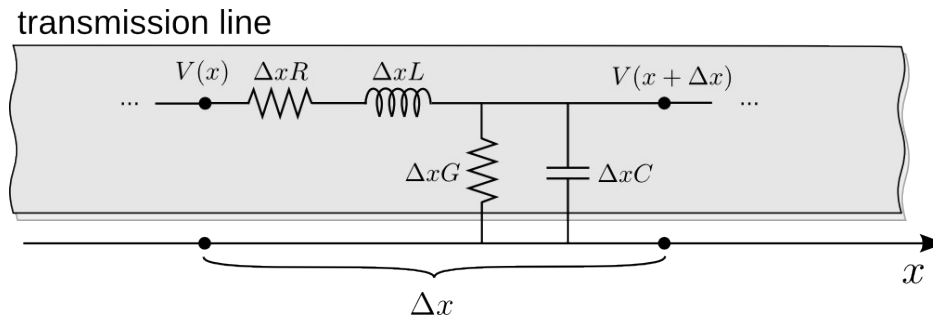
Question: Are there quantum mechanics problems that can be studied experimentally more easily in μw circuits than in a quantum optics setup ?

Circuit model for a transmission line

classical description

- Lumped-element circuit model → size of elements small compared to the wavelength
- This is not true for a waveguide, where the electromagnetic field varies along the length of the waveguide.
- Obtain a lumped-element model by dividing the waveguide in many small parts:

Lossless transmission line (e.g. superconducting)



L = inductance per unit length

C = capacitance per unit length

R = resistance per unit length → 0

G = conductance of dielectric per unit length → 0

Telegrapher's equations:

$$\frac{\partial}{\partial x} V(x, t) = -L \frac{\partial}{\partial t} I(x, t) - RI(x, t)$$

$$\frac{\partial}{\partial x} I(x, t) = -C \frac{\partial}{\partial t} V(x, t) - GV(x, t)$$

Wave equation:

$$\frac{\partial^2}{\partial t^2} V(x, t) = \frac{1}{LC} \frac{\partial^2}{\partial x^2} V(x, t)$$

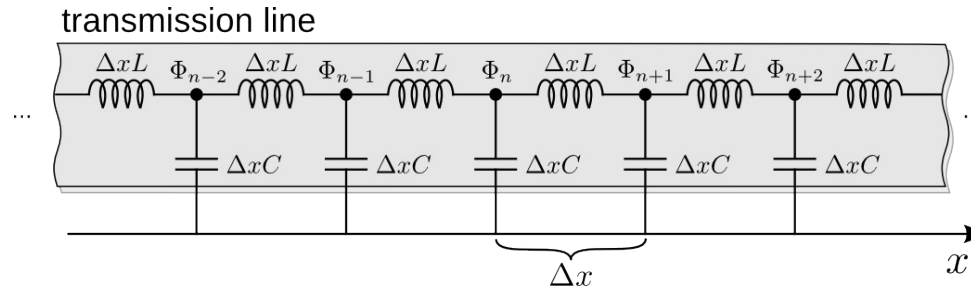
Circuit model for a transmission line

quantum mechanical description

- For later convenience, use magnetic flux instead of voltage:

$$\Phi(x, t) = \int^t dt' V(x, t') \quad \varphi = 2\pi\Phi/\Phi_0$$

- Divide the transmission line in small segments:



- Construct the circuit Lagrangian and Hamiltonian, conjugate variables with canonical commutation relation: $[\Phi_n, P_n] = i\hbar, P_n = \partial\mathcal{L}/\partial\dot{\Phi}_n$

$$\mathcal{L} = \sum_n \left(\frac{1}{2} \Delta x C \dot{\Phi}_n^2 - \frac{1}{2} \frac{1}{\Delta x L} (\Phi_{n+1} - \Phi_n)^2 \right) \quad H = \sum_n \frac{\partial\mathcal{L}}{\partial\dot{\Phi}_n} \dot{\Phi}_n - \mathcal{L}$$

- Continuum limit $\Delta x \rightarrow 0$

$$H = \frac{1}{2} \int dx \left(C [\partial_t \Phi(x, t)]^2 + \frac{1}{L} [\partial_x \Phi(x, t)]^2 \right) \quad \partial_{tt} \Phi(x, t) - \frac{1}{LC} \partial_{xx} \Phi(x, t) = 0$$

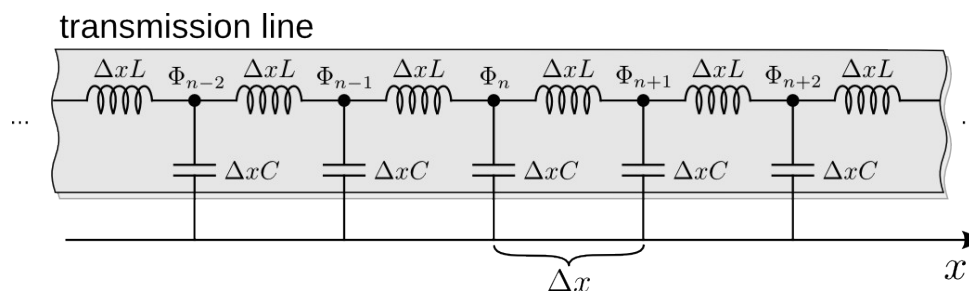
Circuit model for a transmission line

quantum mechanical description

- For later convenience, use magnetic flux instead of voltage:

$$\Phi(x, t) = \int^t dt' V(x, t') \quad \varphi = 2\pi\Phi/\Phi_0$$

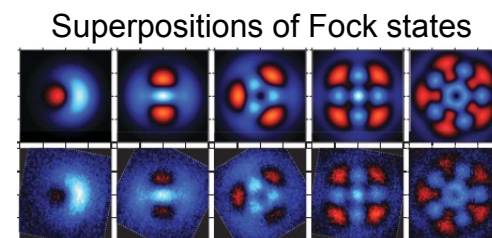
- Divide the transmission line in small segments:



- Quantized flux field $[a(\omega'), a^\dagger(\omega'')] = \delta(\omega' - \omega'')$

$$\Phi(x, t) = \sqrt{\frac{\hbar Z_0}{4\pi}} \int \frac{d\omega}{\sqrt{\omega}} \left(a_L(\omega) e^{-i(+k_\omega x + \omega t)} + a_R(\omega) e^{-i(-k_\omega x + \omega t)} + \text{h.c.} \right)$$

Is a quantum model
of the waveguide
justified/necessary?

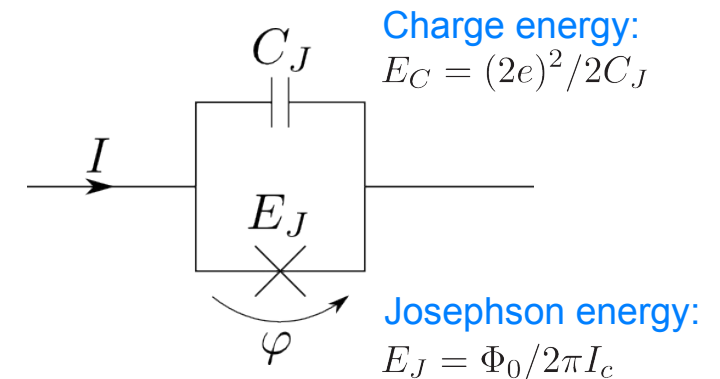
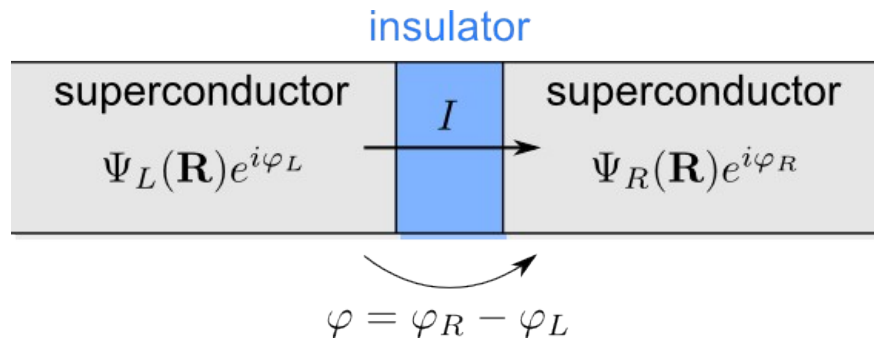


Josephson junction

- A weak tunnel junction between two superconductors

$$\left. \begin{array}{l} \text{phase } \varphi \\ \text{flux } \Phi \end{array} \right\} \varphi = 2\pi \frac{\Phi}{\Phi_0}$$

- non-linear phase-current relation $I = I_c \sin \varphi$
- low dissipation

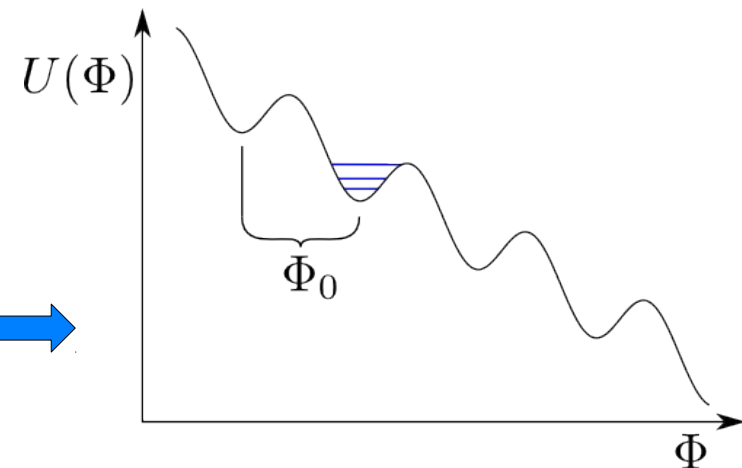
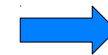


Equation of motion:

$$I = I_c \sin(2\pi\Phi/\Phi_0) + C_J \ddot{\Phi}$$

Lagrangian:

$$L = \underbrace{\frac{1}{2} C_J \dot{\Phi}^2}_{\text{kinetic}} + \underbrace{I\Phi + E_J \cos(2\pi\Phi/\Phi_0)}_{\text{potential}}$$

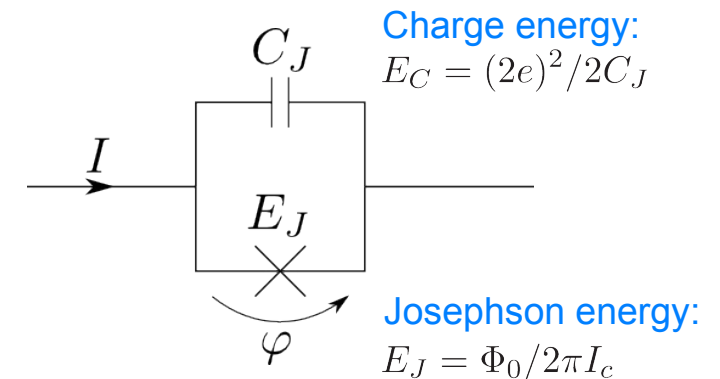
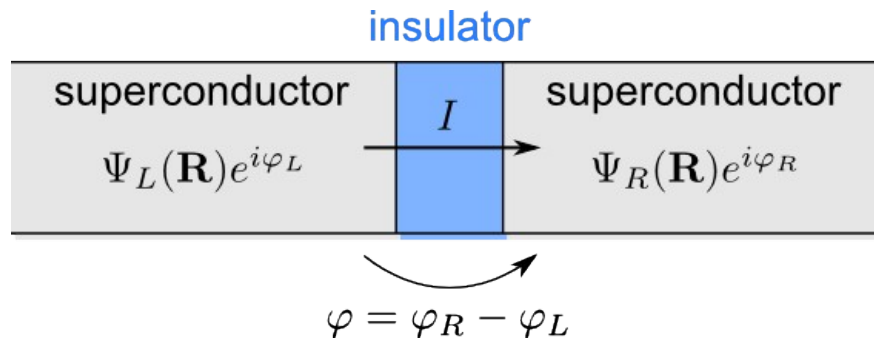


Josephson junction

- A weak tunnel junction between two superconductors

$$\left. \begin{array}{l} \text{phase } \varphi \\ \text{flux } \Phi \end{array} \right\} \varphi = 2\pi \frac{\Phi}{\Phi_0}$$

- non-linear phase-current relation $I = I_c \sin \varphi$
- low dissipation



- Canonical quantization

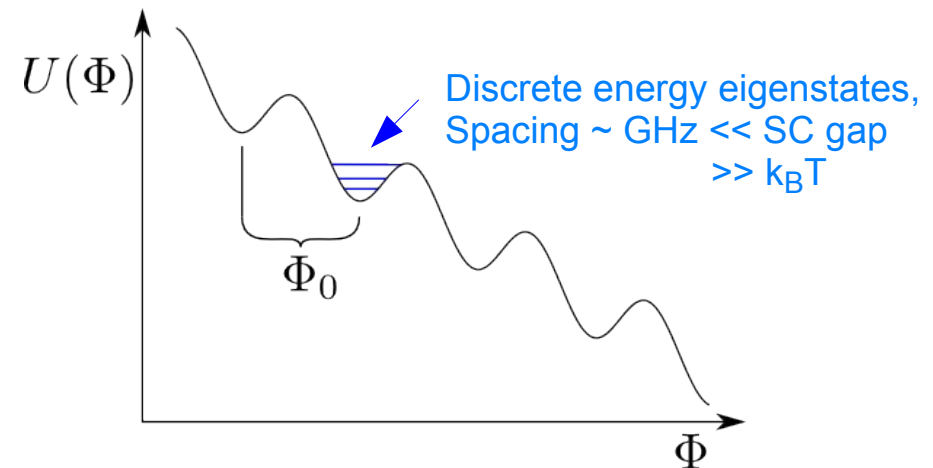
→ conjugate variables: **phase and charge**

$$\frac{E_C}{E_J} \rightarrow \text{Well-defined charge or phase?}$$

- If $E_C \ll E_J$ (phase regime) and small current

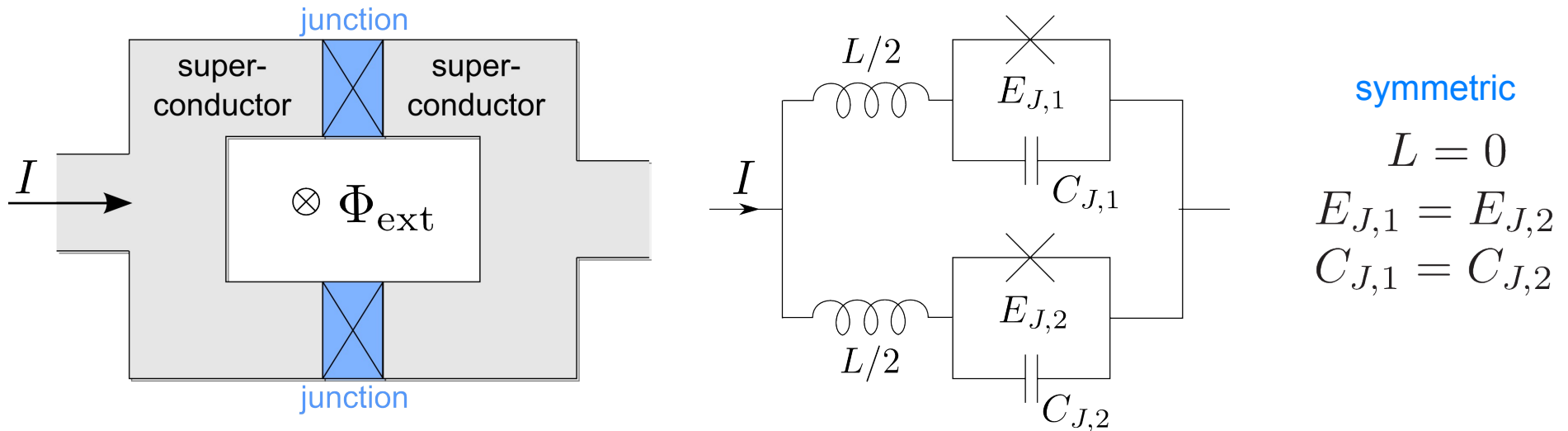
→ **inductance:** $L_J = \left(\frac{\Phi_0}{2\pi}\right)^2 \frac{1}{E_J \cos(\varphi)}$

valid for frequencies smaller than the **plasma frequency:** $\omega_p = \sqrt{2E_J E_C} / \hbar$



SQUID: Superconducting Quantum Interference Device

- A dc-SQUID consists of two Josephson junctions embedded in a superconducting loop



- Fluxoid quantization: single-valuedness of the phase around the loop

$$2\pi \frac{\Phi_{\text{ext}}}{\Phi_0} + \varphi_1 + \varphi_2 = 2\pi n$$

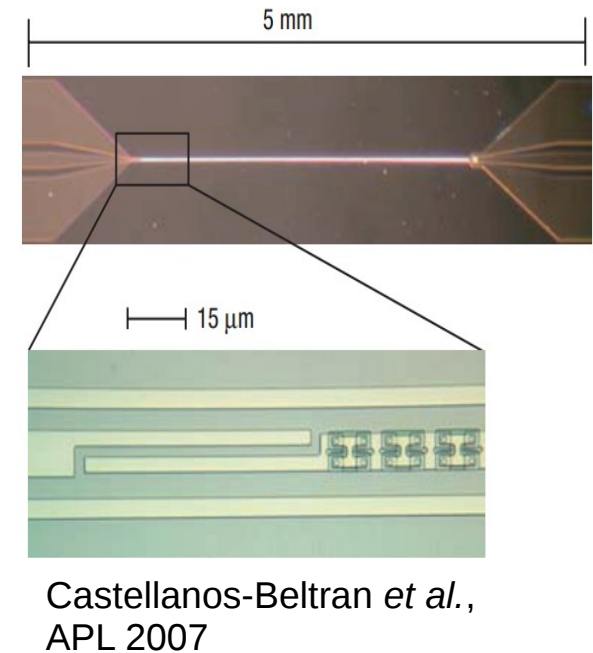
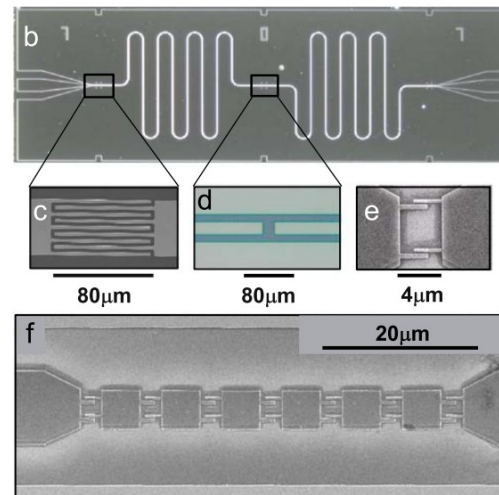
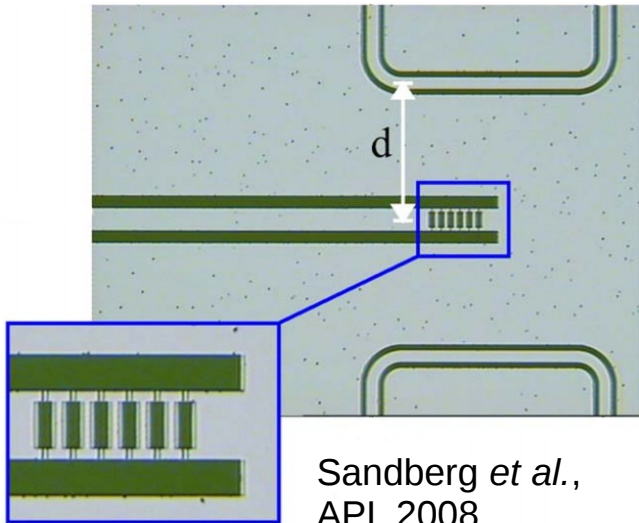
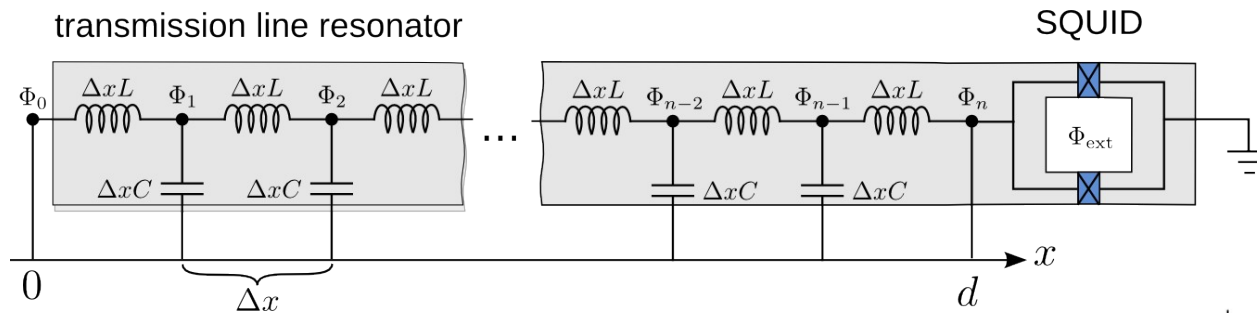
- Behaves as a single Josephson junction, with *tunable* Josephson energy.
- In the phase regime, we get a tunable inductor:

$$L(\Phi_{\text{ext}}) = \left(\frac{\Phi_0}{2\pi} \right)^2 \frac{1}{2E_J \cos(\pi\Phi_{\text{ext}}/\Phi_0)}$$

↑ (tunable)

Frequency tunable resonators

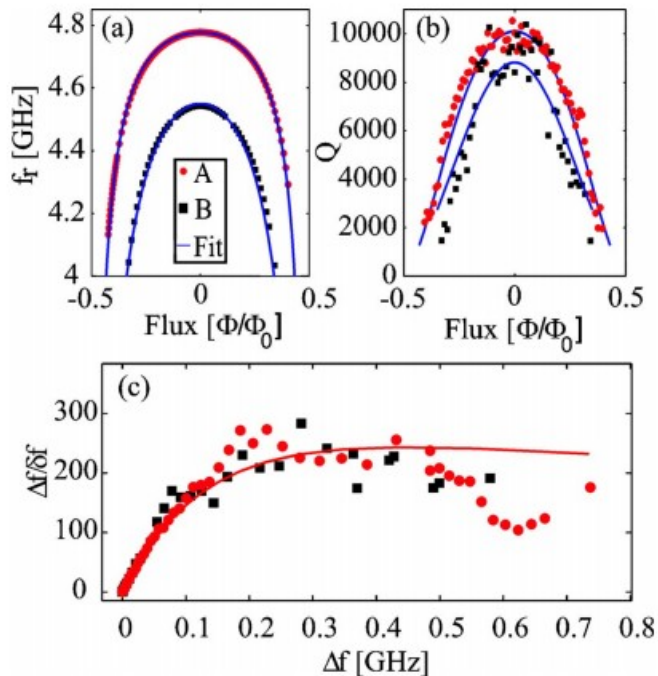
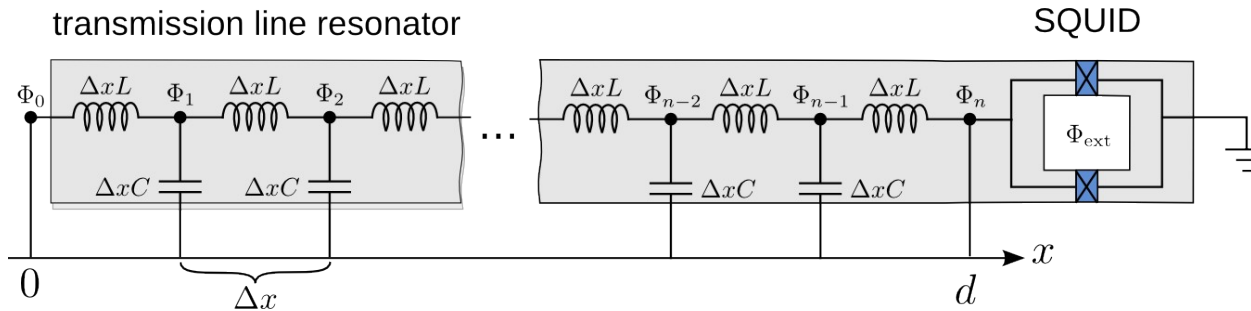
SQUID-terminated transmission line: Wallquist et al. PRB 74 224506 (2006)



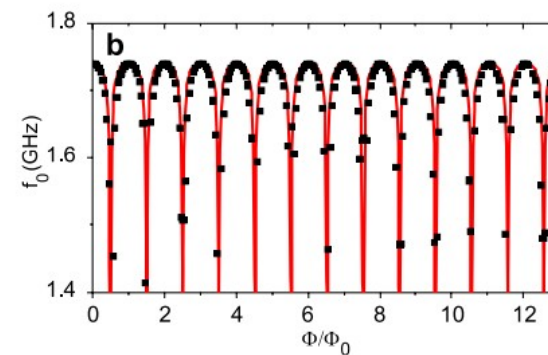
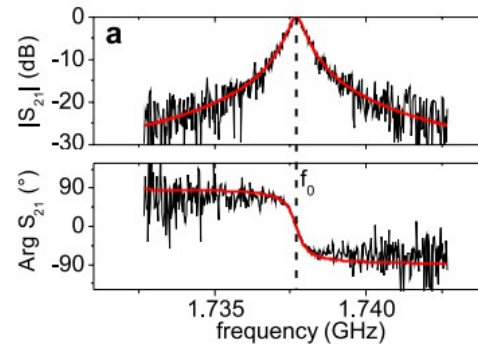
See also:
Yamamoto *et al.*, APL 2008
Kubo *et al.*, PRL 105 140502 (2010)
Wilson *et al.*, PRL 105 233907 (2010)

Frequency tunable resonators

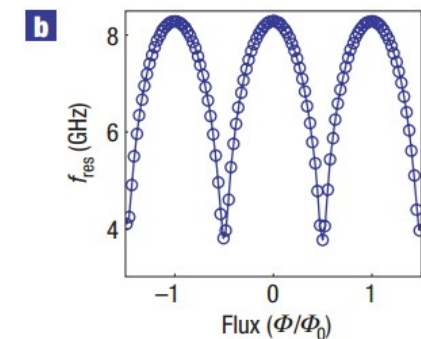
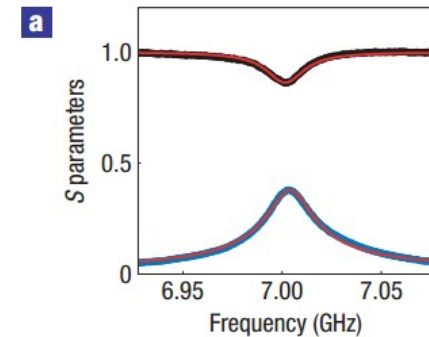
SQUID-terminated transmission line: Wallquist et al. PRB 74 224506 (2006)



Sandberg et al.,
APL 2008



Palacios-Laloy et al.,
JLTP 2008



Castellanos-Beltran et al.,
APL 2007

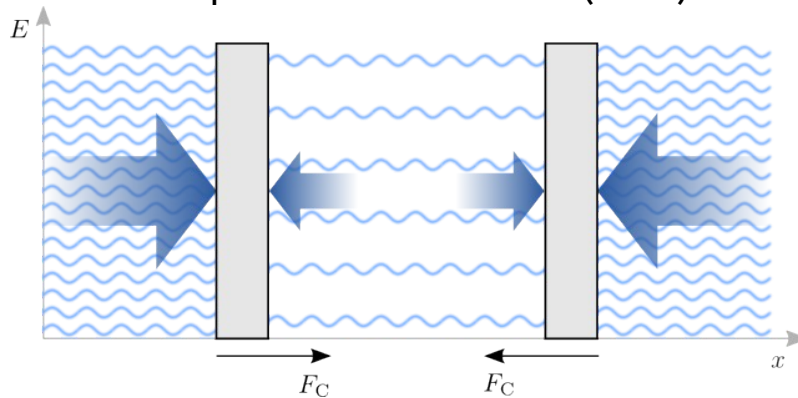
Content

- Quantum optics in superconducting circuits
- [Overview of quantum vacuum effects](#)
- Dynamical Casimir effect in superconducting circuits
- Review of experimental results
- Summary

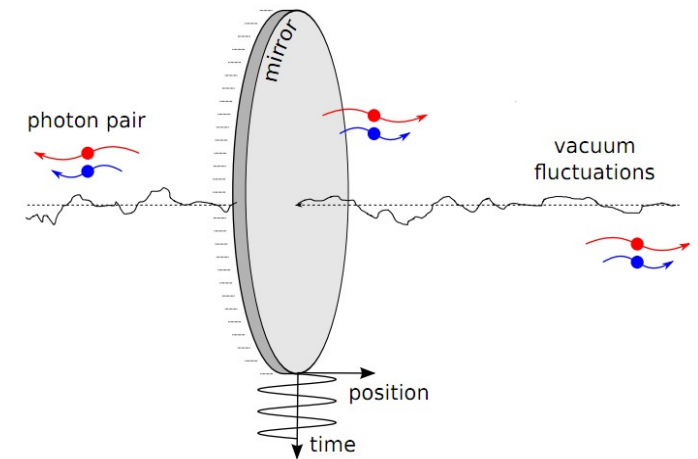
Quantum vacuum effects

Examples of physical phenomena due to quantum vacuum fluctuations (with no classical counterparts).

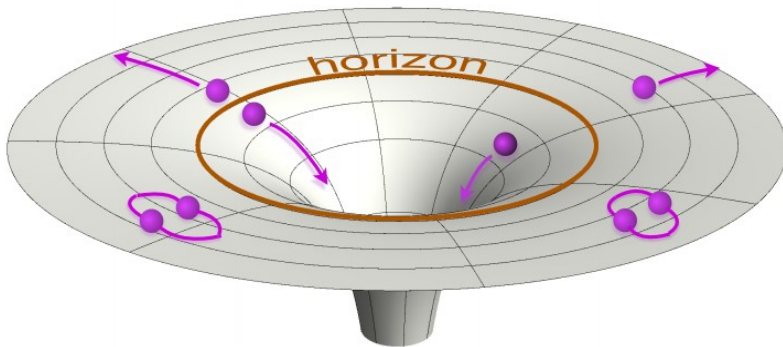
Casimir force (1948)
Experiment: Lamoreaux (1997)



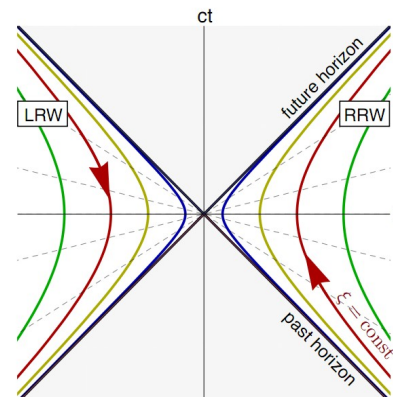
Dynamical Casimir effect



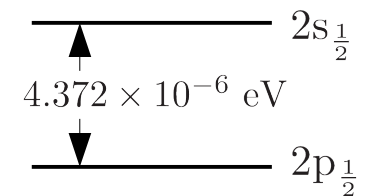
Hawking Radiation



Unruh effect



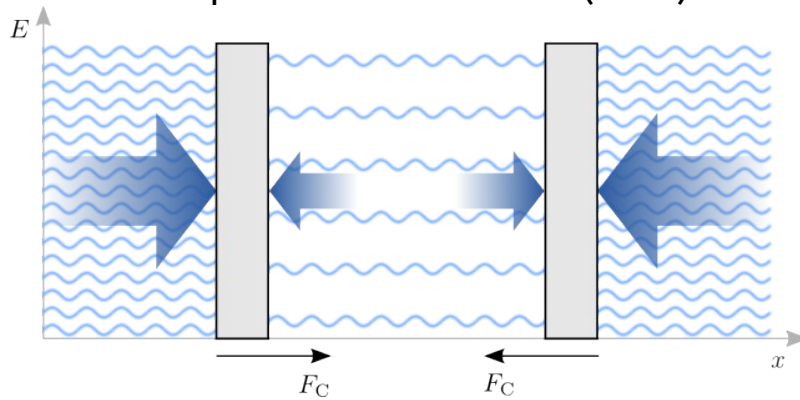
Lamb shift
(Lamb & Retherford 1947)



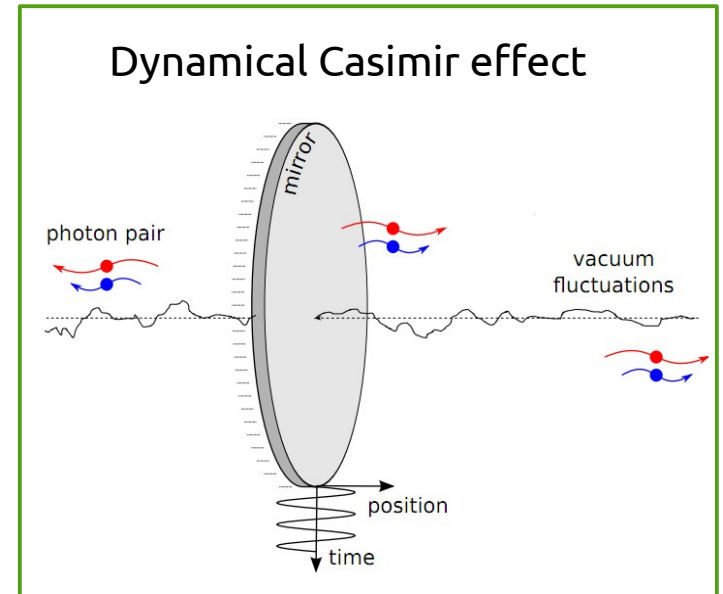
Quantum vacuum effects

Examples of physical phenomena due to quantum vacuum fluctuations (with no classical counterparts).

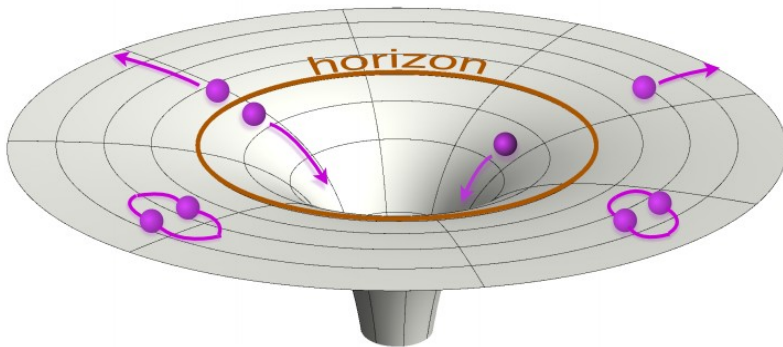
Casimir force (1948)
Experiment: Lamoreaux (1997)



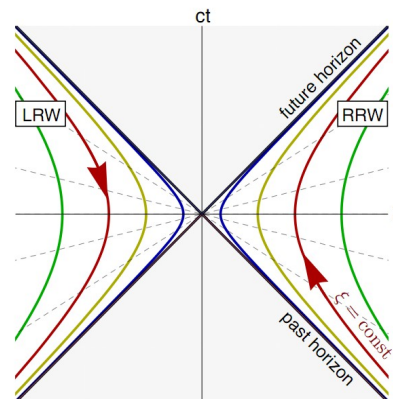
Dynamical Casimir effect



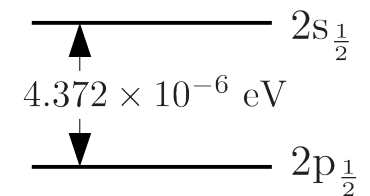
Hawking Radiation



Unruh effect



Lamb shift
(Lamb & Retherford 1947)



The dynamical Casimir effect

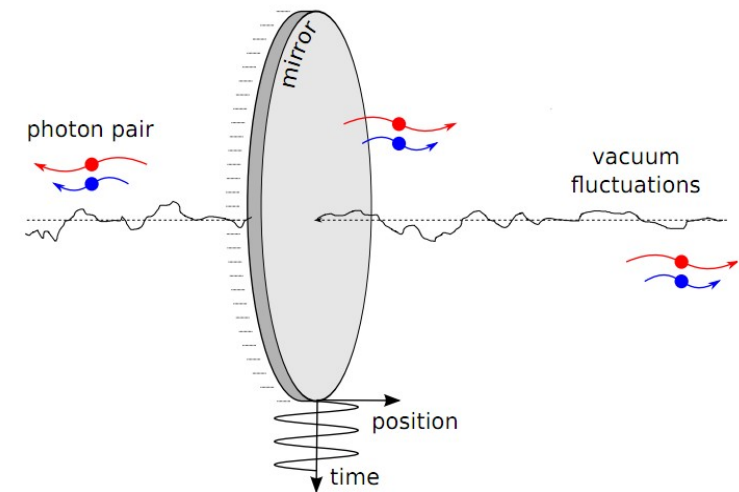
Moore (1970), Fulling (1976)

- *A mirror undergoing nonuniform relativistic motion in vacuum emits radiation*
- In general:

Rapidly changing boundary conditions or index of refraction of a quantum field can modify the mode structure of quantum field **nonadiabatically**, resulting in amplification of virtual photons into real detectable photons (radiation).

- Examples of possible realizations:
 - Moving mirror in vacuum (mentioned above)
 - Medium with time-dependent index of refraction (Yablanovitch 1989, Segev et al 2007)
 - Semiconducting switchable mirror by laser irradiation (Braggio et al 2005, Agnesi et al 2008 & 2011, Naylor et al 2009 & 2012)
 - **Our proposal:**
Superconducting waveguide terminated by a SQUID
(PRL 2009, PRA 2010, experiment Wilson Nature 2011, review Nation RMP 2012)

Dynamical Casimir effect cartoon



Single-mirror photon production rate:

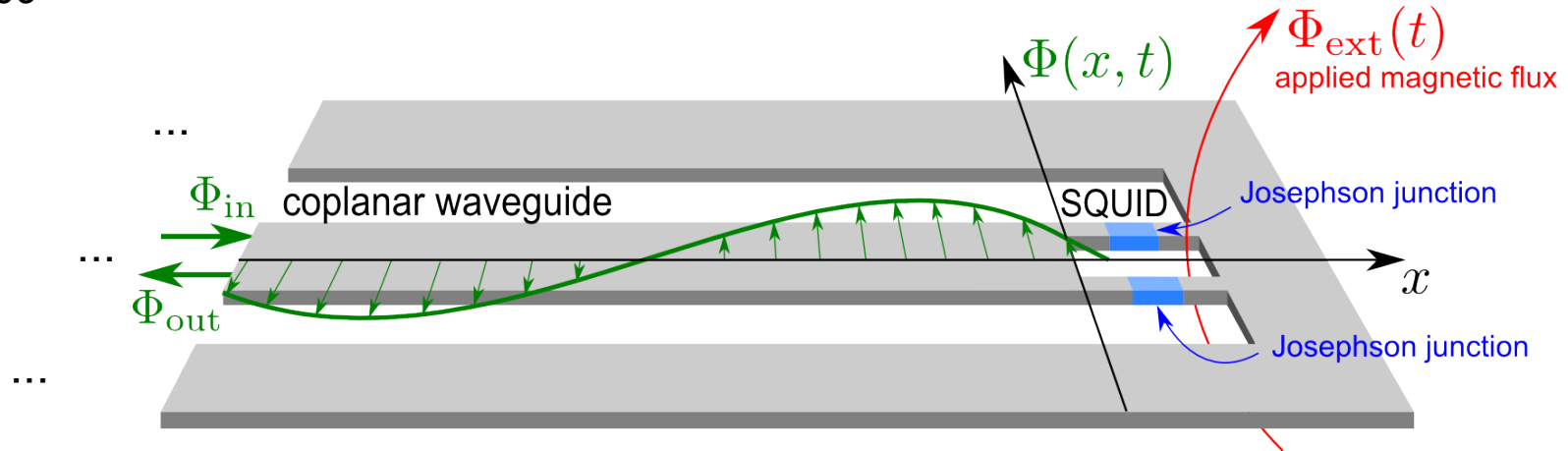
$$\frac{N}{\tau} = \frac{\Omega}{6\pi} \left(\frac{v}{c}\right)^2$$

Content

- Quantum optics in superconducting circuits
- Overview of quantum vacuum effects
- [Dynamical Casimir effect in superconducting circuits](#)
- Review of experimental results
- Summary

Superconducting circuit for DCE

PRL 2009



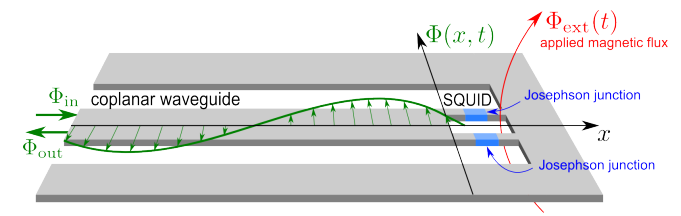
The boundary condition (BC) of the coplanar waveguide (at $x=0$):

- is determined by the SQUID
- can be tuned by the **applied magnetic flux** through the SQUID
- is effectively equivalent to a “mirror” with tunable position (1-to-1 mapping of BC)
- harmonic modulation of the applied magnetic flux results in DCE radiation.

Tunable resonators:
Sandberg (2008)
Palacios-Laloy (2008)
Yamamoto (2008)

No motion of massive objects is involved in this method of changing the boundary condition.

Circuit model

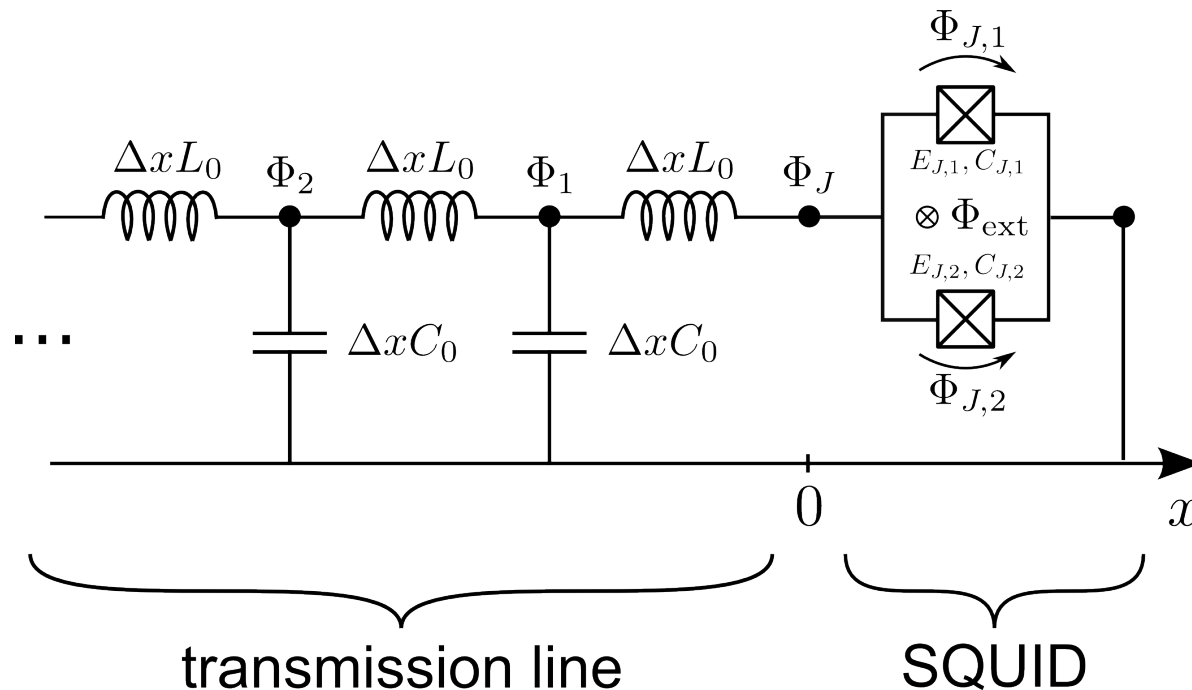


Circuit model of the coplanar waveguide and the SQUID

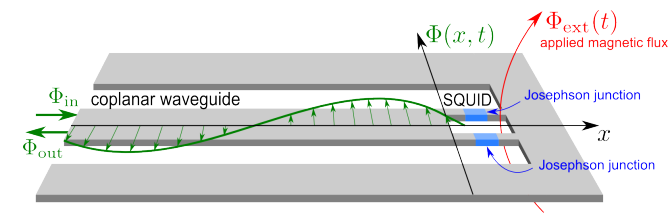
- Symmetric SQUID with negligible loop inductance:

$$E_{J,1} = E_{J,2}, \quad C_{J,1} = C_{J,2}$$

$$L = 0 \quad \Rightarrow \quad \Phi_{J,1} - \Phi_{J,2} = \Phi_{\text{ext}}$$



Circuit model



Circuit model of the coplanar waveguide and the SQUID

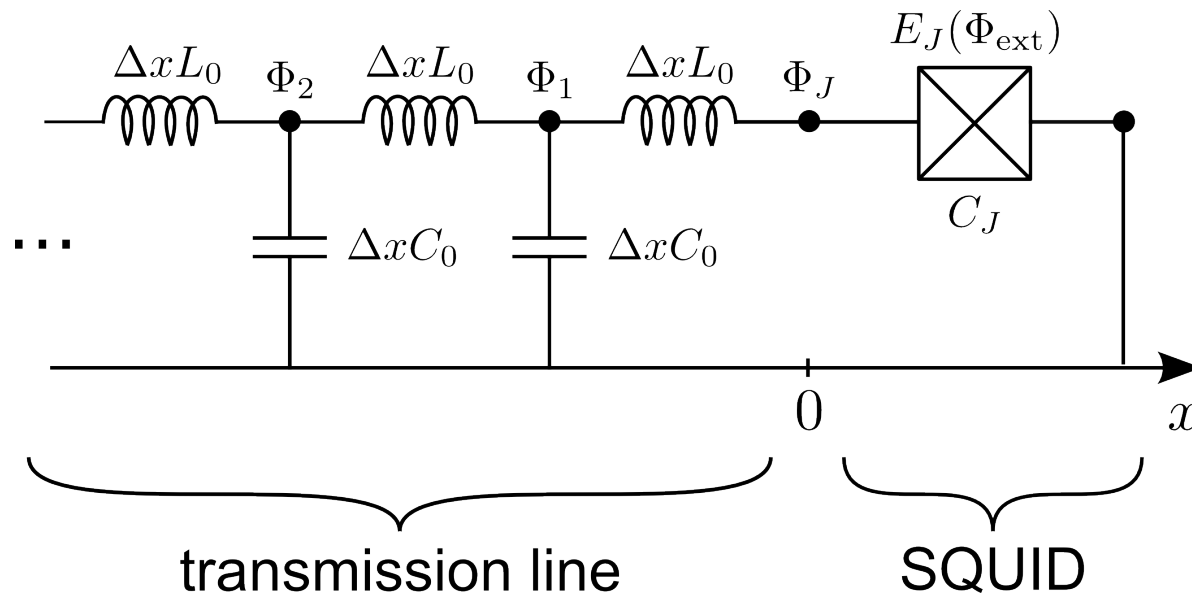
- Symmetric SQUID with negligible loop inductance:

$$E_{J,1} = E_{J,2}, \quad C_{J,1} = C_{J,2}$$

$$L = 0 \quad \Rightarrow \quad \Phi_{J,1} - \Phi_{J,2} = \Phi_{\text{ext}}$$

- The SQUID behaves as an effective junction with tunable Josephson energy

$$E_J(\Phi_{\text{ext}}) = E_J \sqrt{2 + 2 \cos(2\pi \Phi_{\text{ext}} / \Phi_0)}$$



The boundary condition

Circuit analysis gives:

- Hamiltonian:

$$H = \frac{1}{2} \sum_{i=0}^{\infty} \left(\frac{(P_i)^2}{C_0 \Delta x} + \frac{1}{L_0} \frac{(\Phi_{i+1} - \Phi_i)^2}{\Delta x} \right) + \frac{1}{2} \frac{(P_J)^2}{C_J} - E_J(\Phi_{\text{ext}}(t)) \cos \left(2\pi \frac{\Phi_J}{\Phi_0} \right)$$

- We assume that the SQUID is only weakly excited (large plasma frequency)

$$\cos \left(2\pi \frac{\Phi_J}{\Phi_0} \right) \sim - \left(\frac{2\pi}{\Phi_0} \right)^2 \Phi_J^2$$



- The equation of motion for $\Phi_J \equiv \Phi(x=0, t)$ gives the boundary condition for the transmission line:

$$\left(\frac{2\pi}{\Phi_0} \right)^2 E_J(t) \Phi(0, t) + \frac{1}{L_0} \left. \frac{\partial \Phi(x, t)}{\partial x} \right|_{x=0} + C_J \frac{\partial^2 \Phi(0, t)}{\partial t^2} = 0$$

Quantized field in the coplanar waveguide

The phase field of the transmission line is governed by the *wave equation* and it has independent left and right propagating components:

$$\Phi(x, t) = \sqrt{\frac{\hbar Z_0}{4\pi}} \int_0^\infty \frac{d\omega}{\sqrt{\omega}} \left(a_\omega^{\text{in}} e^{-i(-k_\omega x + \omega t)} + \text{h.c.} \right) + \sqrt{\frac{\hbar Z_0}{4\pi}} \int_0^\infty \frac{d\omega}{\sqrt{\omega}} \left(a_\omega^{\text{out}} e^{-i(+k_\omega x + \omega t)} + \text{h.c.} \right)$$

 propagates to the right along the x-axis
 propagates to the left along the x-axis

a_ω^{in} = annihilation operator for photons propagating to the right

a_ω^{out} = annihilation operator for photons propagating to the left

Z_0 = characteristic impedance of the coplanar waveguide

Insert into the boundary condition and *solve using input-output theory*:

$$\int_{-\infty}^{\infty} d\omega' S(\omega, \omega') \left[\Theta(\omega') (a_{\omega'}^{\text{in}} + a_{\omega'}^{\text{out}}) + \Theta(-\omega') (a_{-\omega'}^{\text{in}} + a_{-\omega'}^{\text{out}})^\dagger \right] + ik_\omega L_{\text{eff}}^0 (a_\omega^{\text{in}} - a_\omega^{\text{out}}) = 0$$

$$S(\omega, \omega') = \frac{1}{2\pi} \sqrt{\frac{\omega}{\omega'}} \int_{-\infty}^{\infty} dt e^{-i(\omega' - \omega)t} E_J(t)$$

$$a_\omega^{\text{out}} = ?$$

Equivalent effective length of the SQUID

Input-output analysis for a *static flux*:

$$a_{\omega}^{\text{out}} = -\frac{1 + ik_{\omega}L_{\text{eff}}^0}{1 - ik_{\omega}L_{\text{eff}}^0} a_{\omega}^{\text{in}} \equiv R(\omega) a_{\omega}^{\text{in}}$$

$$k_{\omega}L_{\text{eff}}^0 \ll 1$$

$$R_{\text{SQUID}}(\omega) \approx -e^{2ik_{\omega}L_{\text{eff}}^0}$$

$$R_{\text{mirror}}(\omega) \approx -e^{2ik_{\omega}L}$$

Physical interpretation of the effective length

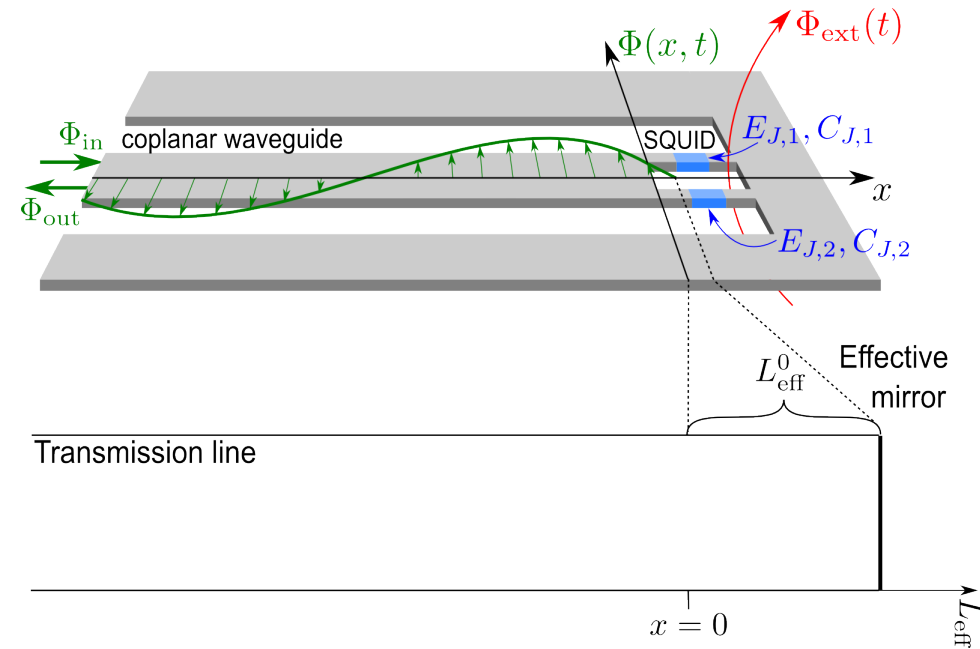
- The effective length is defined as

$$L_{\text{eff}}(t) = \left(\frac{\Phi_0}{2\pi} \right)^2 \frac{1}{L_0 E_J(t)}$$

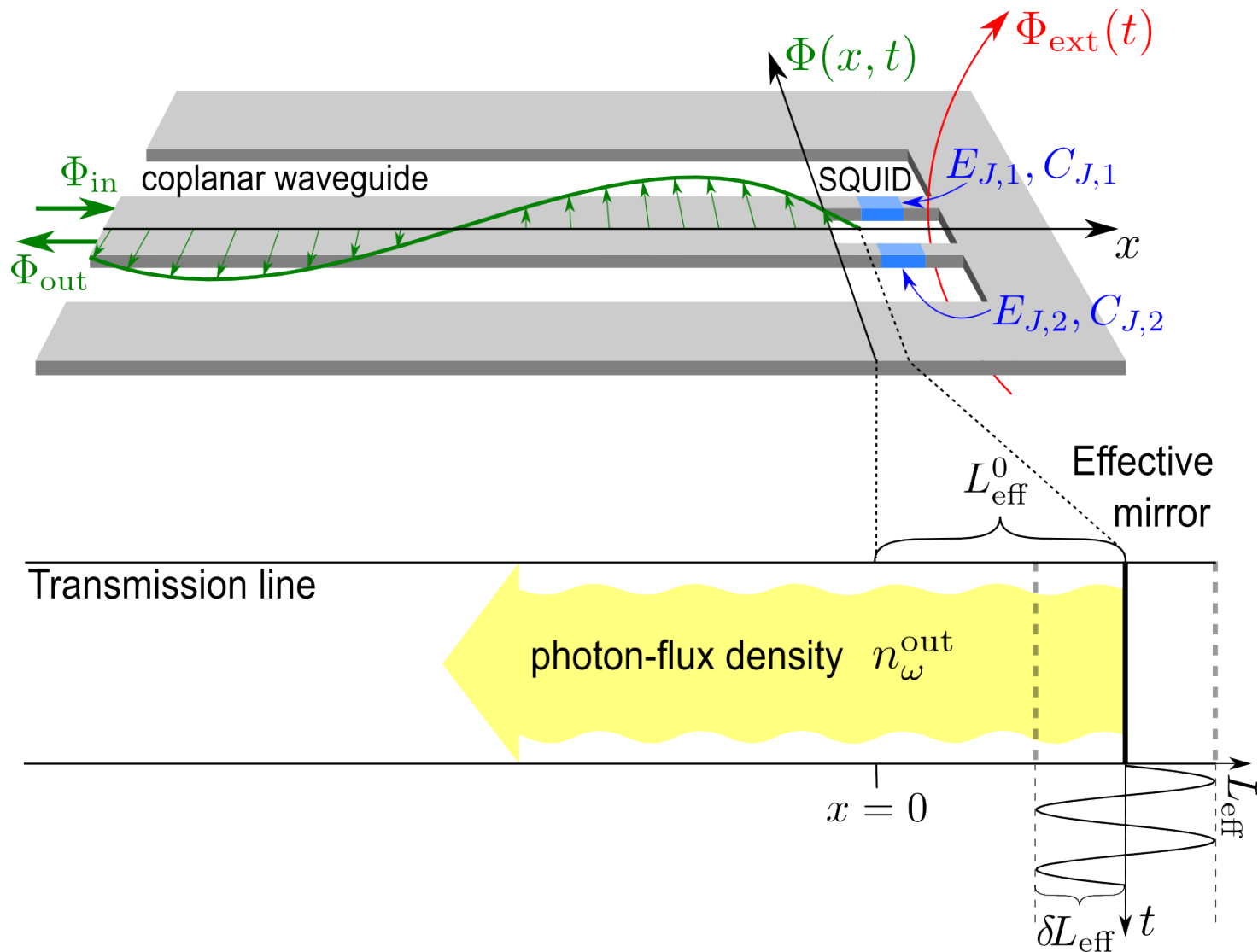
- Can be interpreted as the distance to an “effective mirror”, i.e., to the point where the field is zero.
- With identical scattering properties.

Effective length of SQUID:

function of the Josephson energy, or the applied magnetic flux → *tunable!*

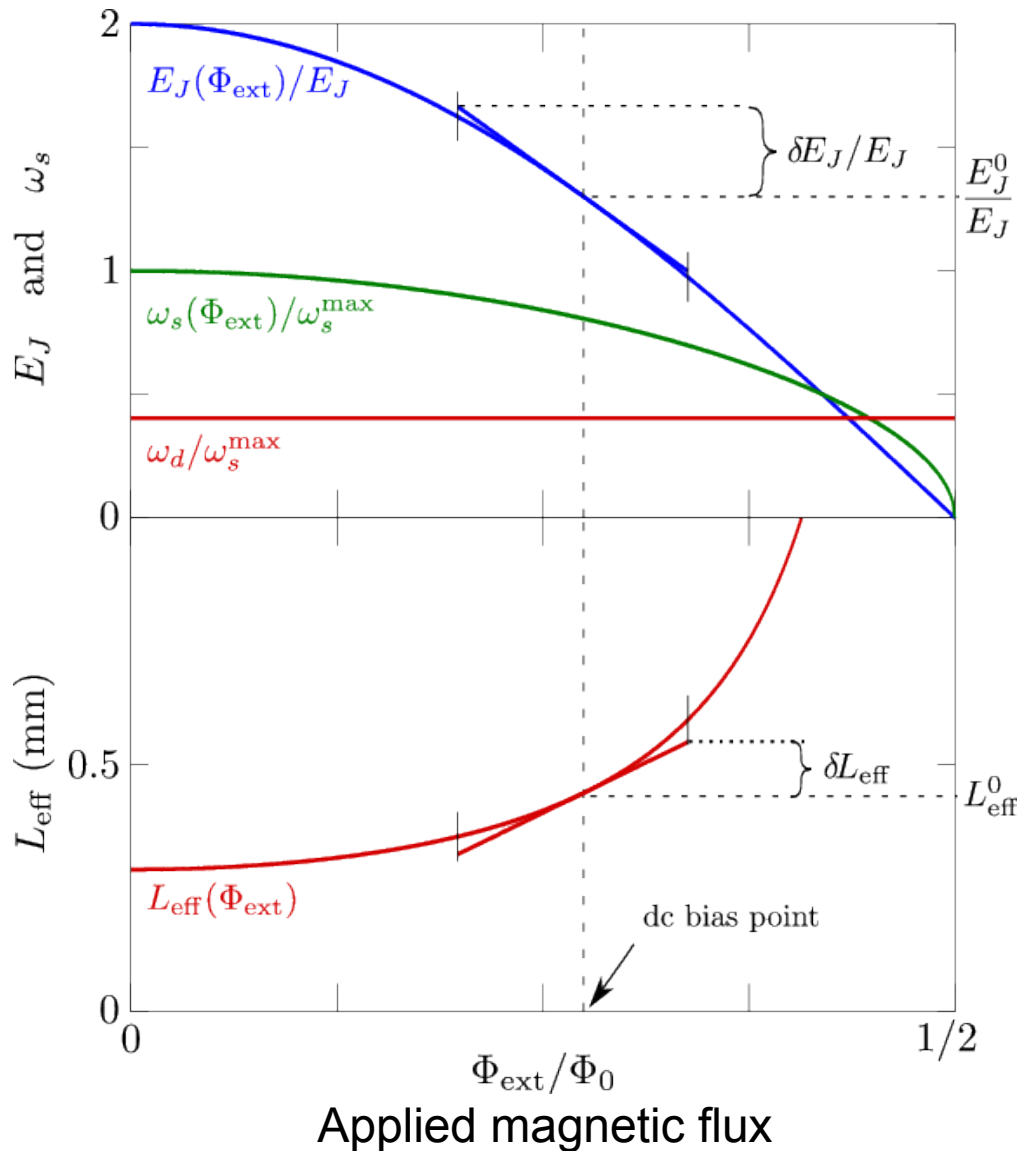


Oscillating boundary condition



Effective-length vs. applied magnetic flux

Modulating the applied magnetic flux → modulated effective length



Josephson energy of the SQUID

$$E_J(t) = E_J^0 + \delta E_J \cos(\omega_d t)$$

Effective length

$$L_{\text{eff}} = L_{\text{eff}}^0 + \delta L_{\text{eff}} \cos(\omega_d t)$$

Input-output result for oscillating BC

Perturbation solution for sinusoidal modulation: $L_{\text{eff}} = L_{\text{eff}}^0 + \delta L_{\text{eff}} \cos(\omega_d t)$

$$a_{\text{out}}(\omega) = R(\omega)a_{\text{in}}(\omega) - i \frac{\delta L_{\text{eff}}}{v} \sqrt{\omega(\omega - \omega_d)} a_{\text{in}}(\omega + \omega_d) - i \frac{\delta L_{\text{eff}}}{v} \sqrt{\omega|\omega - \omega_d|} \left[a_{\text{in}}(\omega - \omega_d) \Theta(\omega - \omega_d) + a_{\text{in}}^\dagger(\omega_d - \omega) \Theta(\omega_d - \omega) \right]$$

$v = \frac{1}{\sqrt{L_0 C_0}}$ = speed of light in the coplanar waveguide

$\Theta(\omega)$ = the Heaviside step function

Now any expectation values and correlation functions for the output field can be calculated:

$$\langle f(a_{\text{out}}(\omega), a_{\text{out}}(\omega'), \dots) \rangle = \dots$$

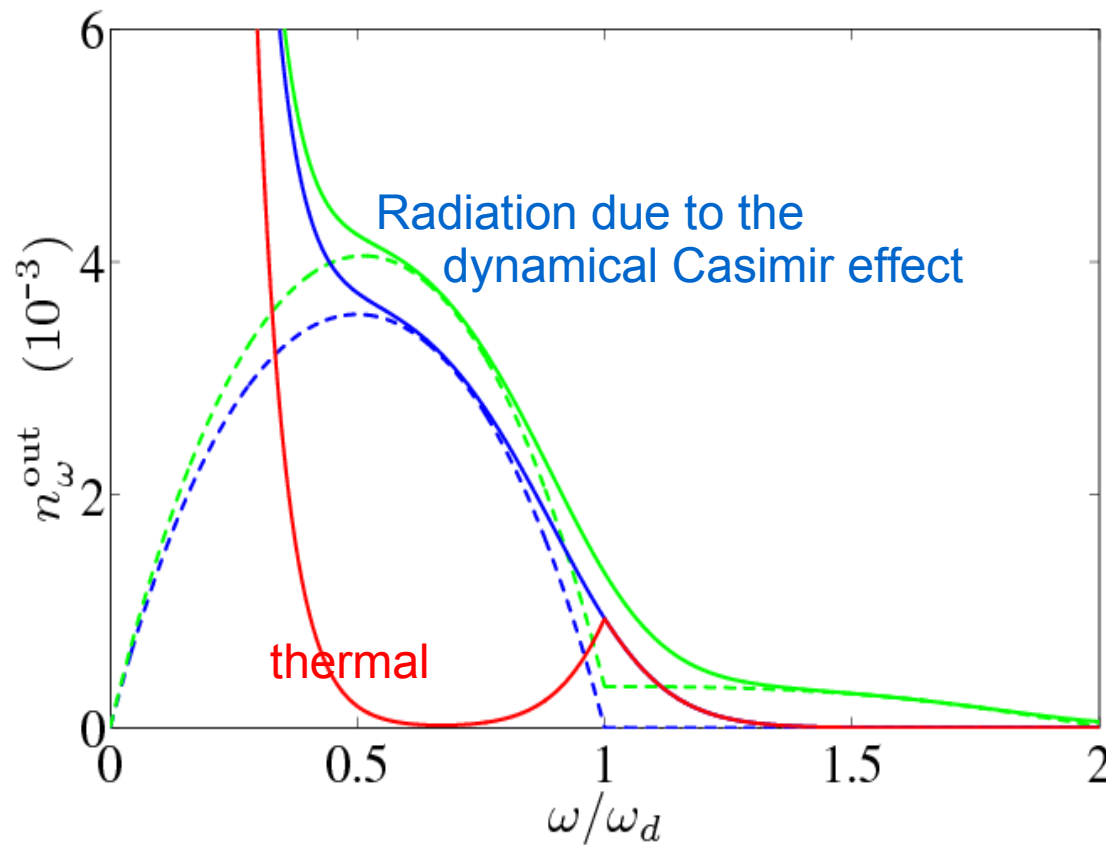
For example, the photon flux in the output field for a thermal input field:

$$n_{\omega}^{\text{out}} \approx \underbrace{\bar{n}_{\omega}^{\text{in}} + \left(\frac{\delta L_{\text{eff}}}{v} \right)^2 \omega |\omega - \omega_d| \bar{n}_{|\omega - \omega_d|}^{\text{in}}}_{\text{Reflected thermal photons}} + \underbrace{\left(\frac{\delta L_{\text{eff}}}{v} \right)^2 \omega |\omega_d - \omega| \Theta(\omega_d - \omega)}_{\text{Dynamical Casimir effect !}}$$

Example of photon-flux density spectrum

Predicted output photon-flux density vs. mode frequency:

→ broadband photon production below the driving frequency



Red: thermal photons

Blue: analytical results

Green: numerical results

Temperature:

- Solid: $T = 50$ mK

- Dashed: $T = 0$ K

$$\delta E_J \approx E_J^0/4$$

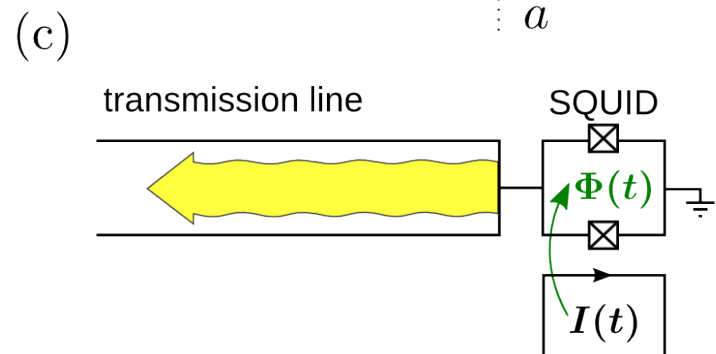
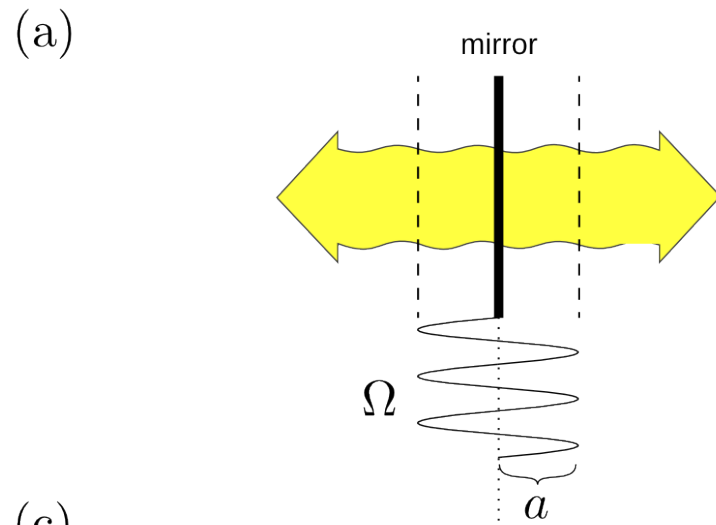
$$\begin{aligned} \omega_p &= 2\pi \sqrt{E_J^0/C\Phi_0^2} \\ &\approx 46\text{GHz} \\ &\text{(plasma frequency)} \end{aligned}$$

$$\begin{aligned} \omega_d &\approx 18\text{GHz} \\ &\text{(driving frequency)} \end{aligned}$$

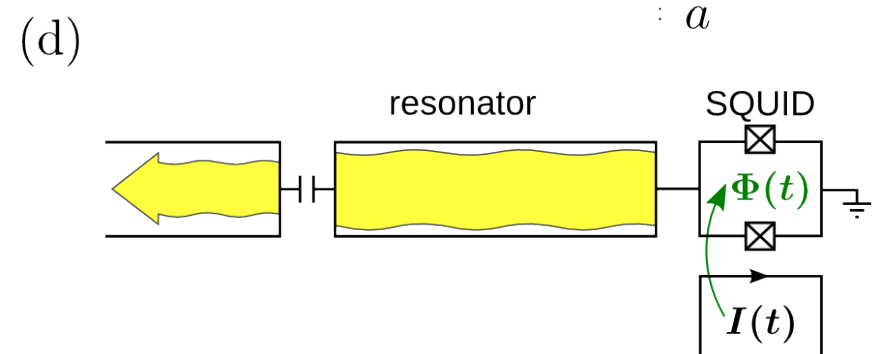
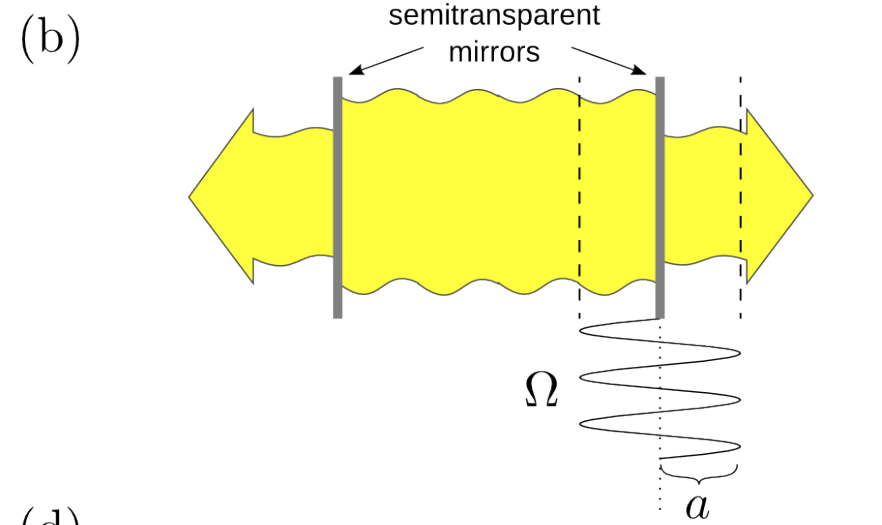
DCE in a cavity/resonator setup

PRA 2010

Single-mirror setups

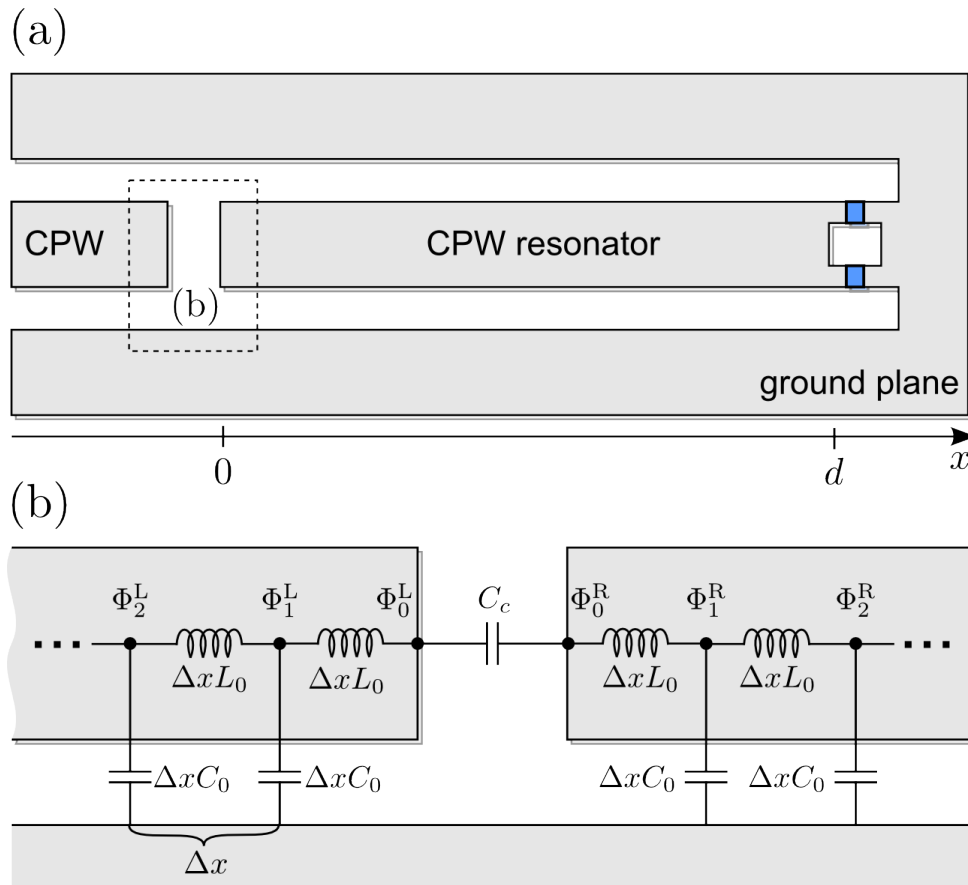


Cavity and resonator setups

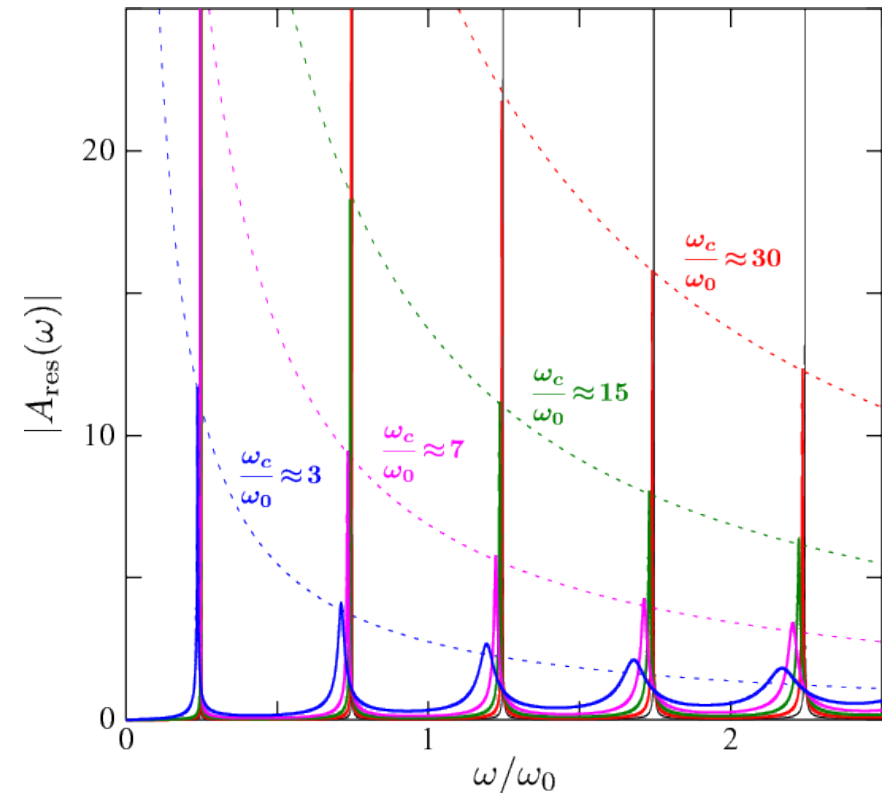


DCE in a SC coplanar waveguide resonator

Resonator circuit:



Resonance spectrum for different Q values

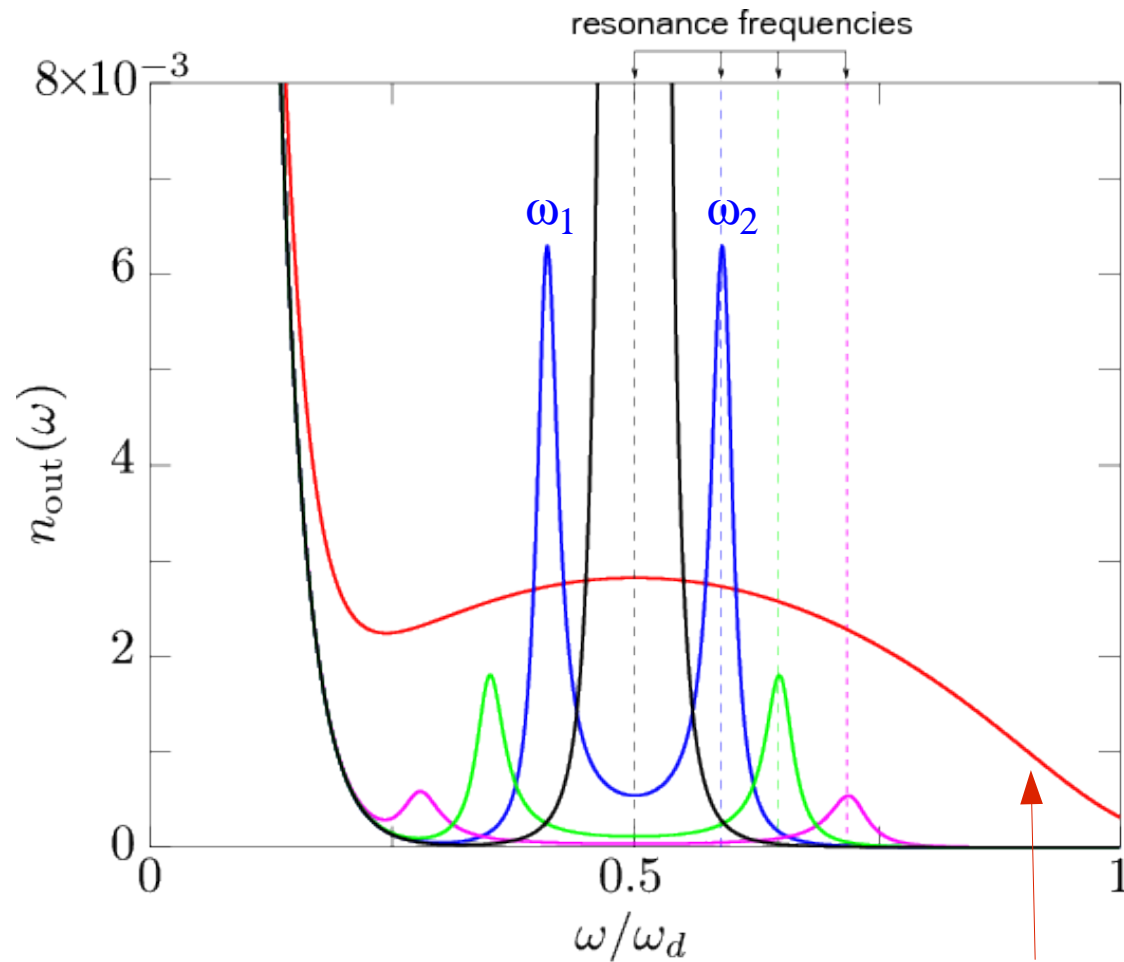


Advantage: On resonance, DCE photons are parametrically amplified

Disadvantage: Harder to distinguish from parametric amplification of thermal photons.

DCE in a SC coplanar waveguide resonator

Photon-flux density for DCE in the resonator setup



Symmetric double-peak structure when the driving frequency ω_d is *detuned* from twice the resonance frequency ω_{res}

The resonator concentrates the DCE radiation in two modes ω_1 and ω_2 that satisfy:

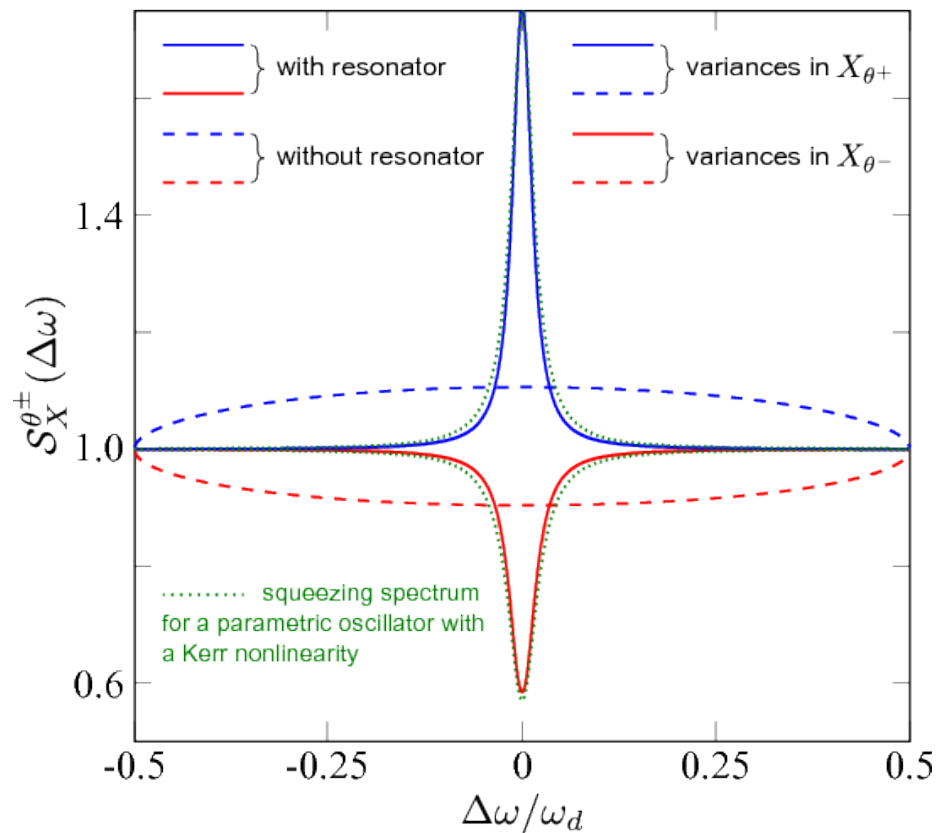
$$\omega_1 + \omega_2 = \omega_d$$

Photons in the ω_1 and ω_2 modes are *correlated*.

Open waveguide case:
single broad peak

Example of two-mode squeezing spectrum

- DCE generates two-mode squeezed states (correlated photon pairs)
- Broadband quadrature squeezing



Advantages:

- Can be measured with standard homodyne detection.
- Photon correlations at different frequencies is a signature of quantum generation process.

Solid lines: Resonator setup
Dashed lines: Open waveguide

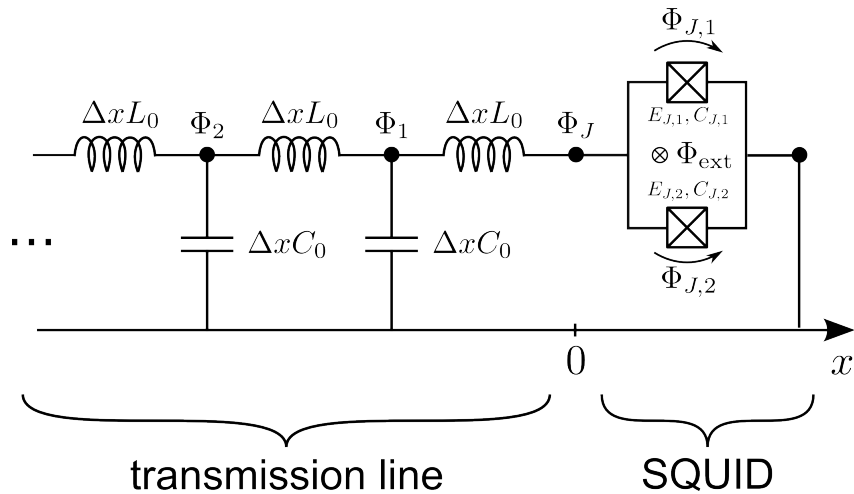
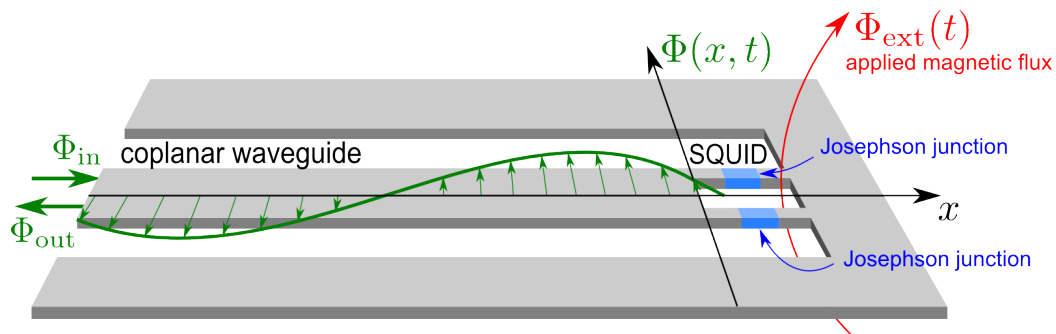
Experimental results

Wilson et al. Nature 2011

Lähteenmäki et al., PNAS (2013)

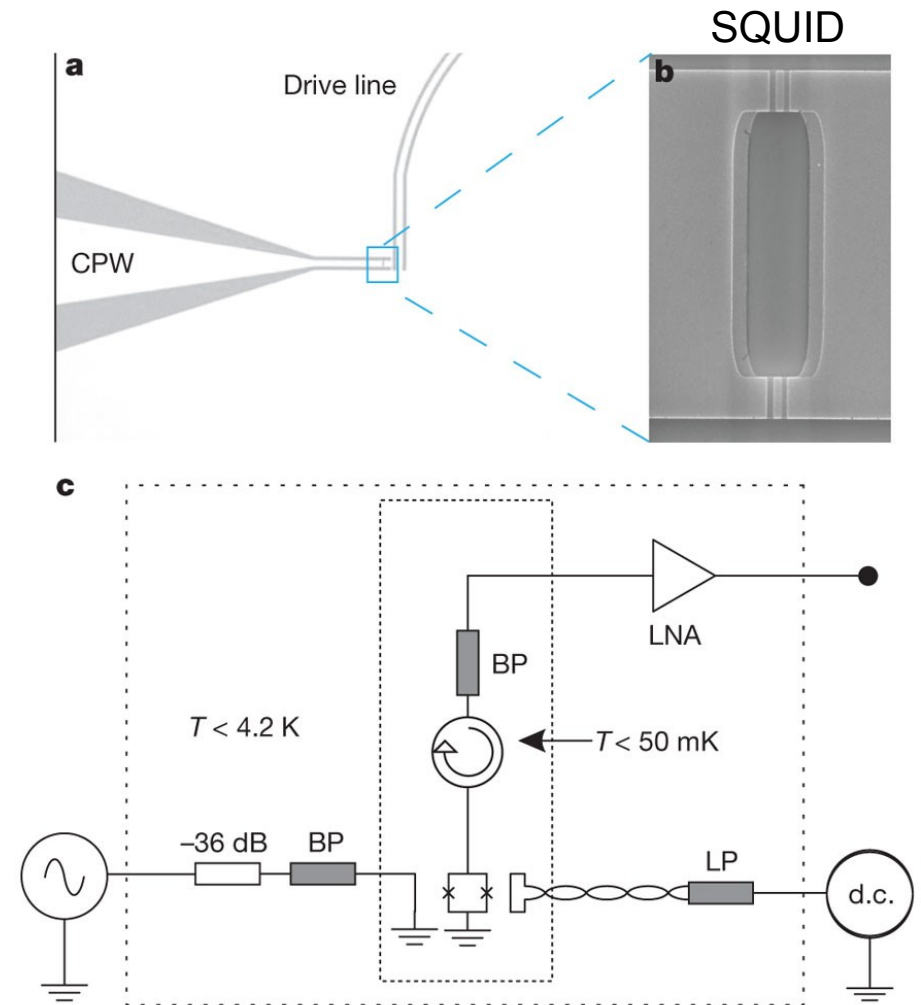
The experimental setup

Schematic



PRL 2009, PRA 2010

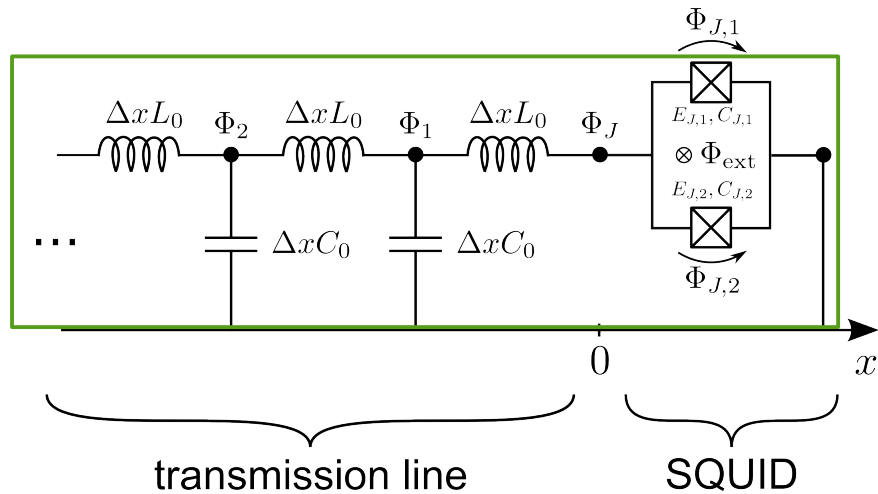
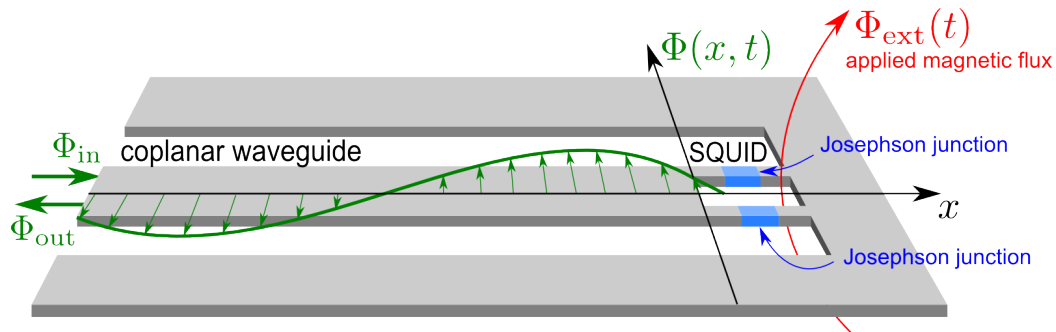
Experiment



Wilson (Nature 2011)

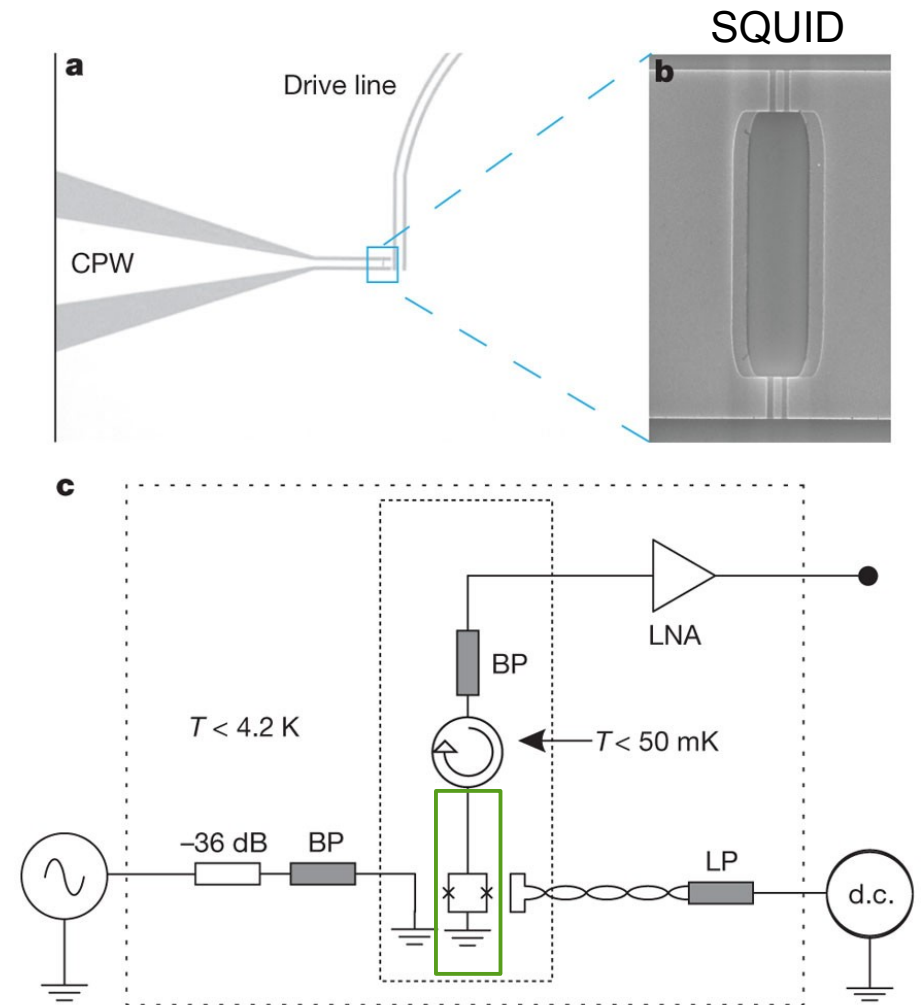
The experimental setup

Schematic



PRL 2009, PRA 2010

Experiment

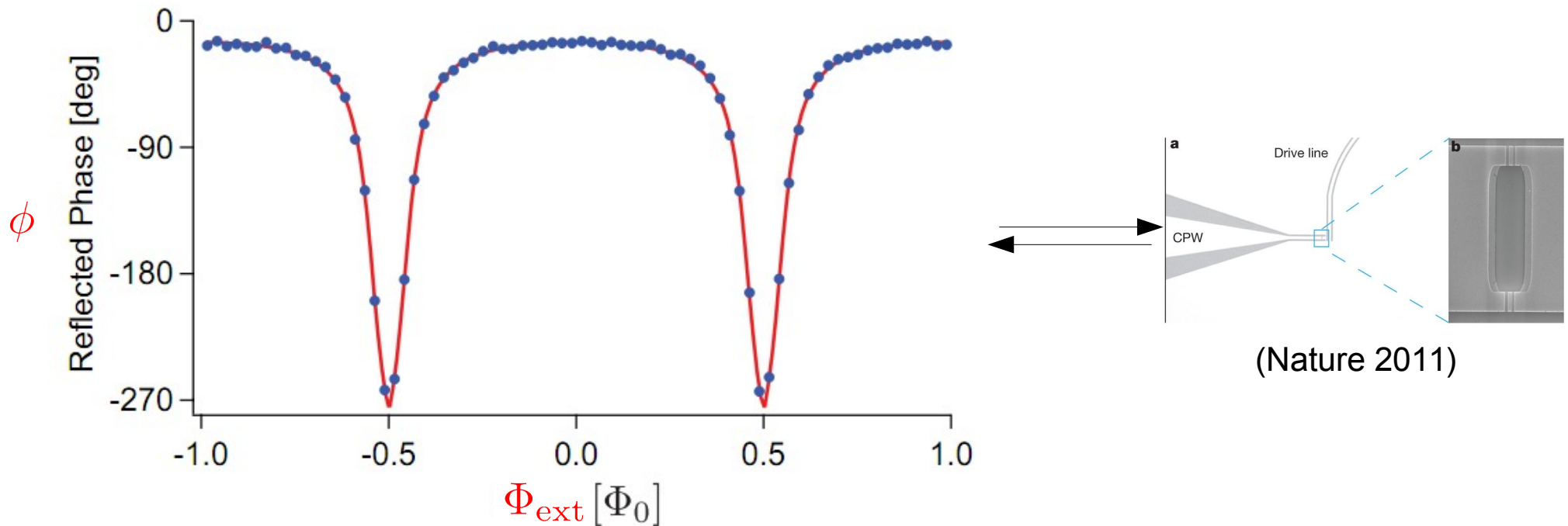


Wilson (Nature 2011)

Measured reflected phase

Testing the tunability of the effective length:

Measurement of the phase acquired by an incoming signal that reflect off the SQUID as a function of the externally applied *static* magnetic field.



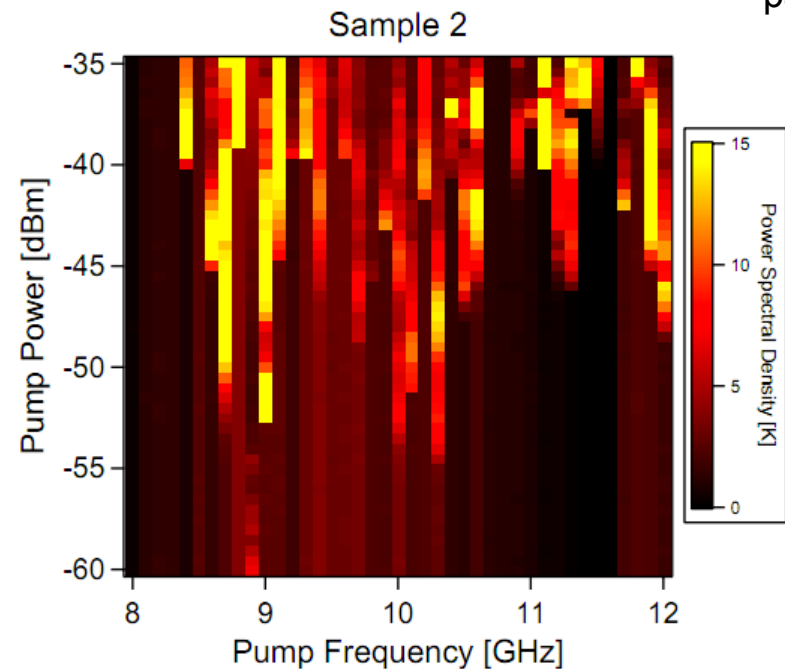
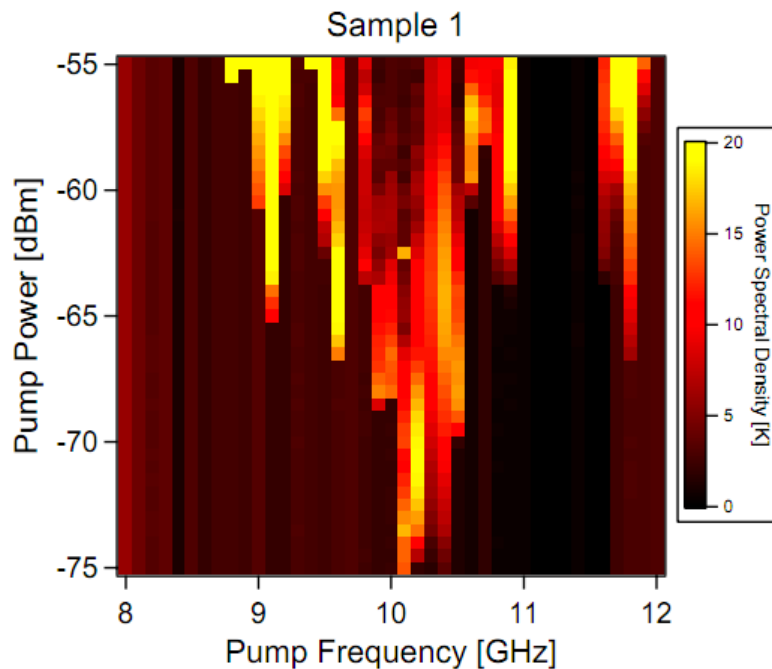
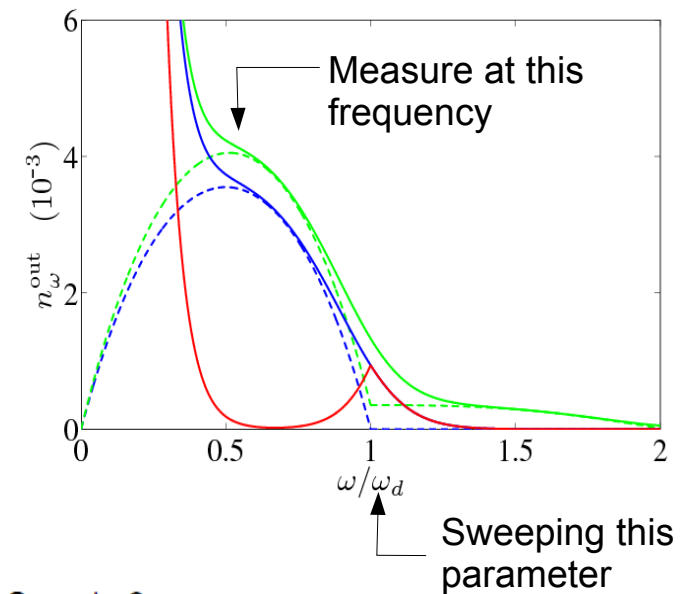
The reflected phase is directly related to the effective “electrical length” of the SQUID.

$$L_{\text{eff}}^0 = \left(\frac{\Phi_0}{2\pi} \right)^2 \frac{1}{L_0 E_J(\Phi_{\text{ext}})}$$

Measured photon-flux density: I

Sweeping the pump frequency and measuring the photon flux at half the driving frequency (where DCE radiation is predicted to peak) as a function of the pump power.

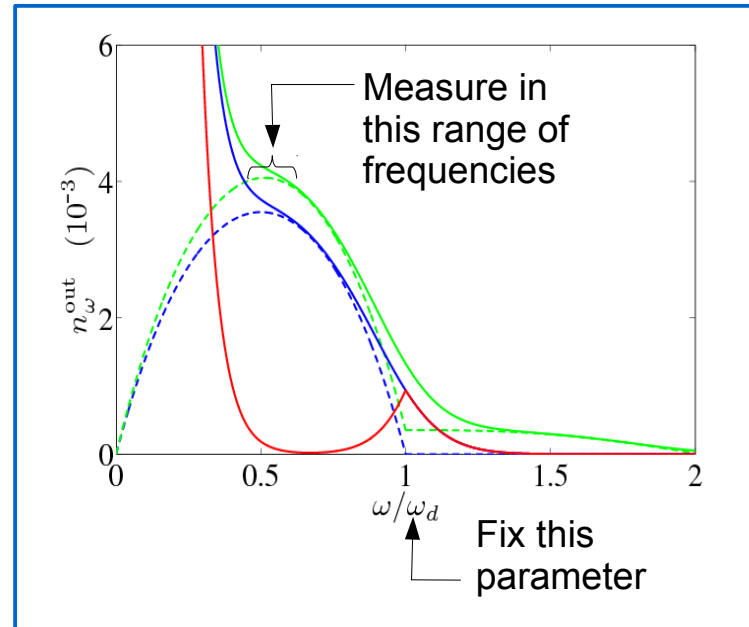
Photon production is observed for all pump frequencies, but the intensity varies significantly due to nonuniformity of the transmission line that connect the circuit and measurement apparatus.



Measured photon-flux density: II

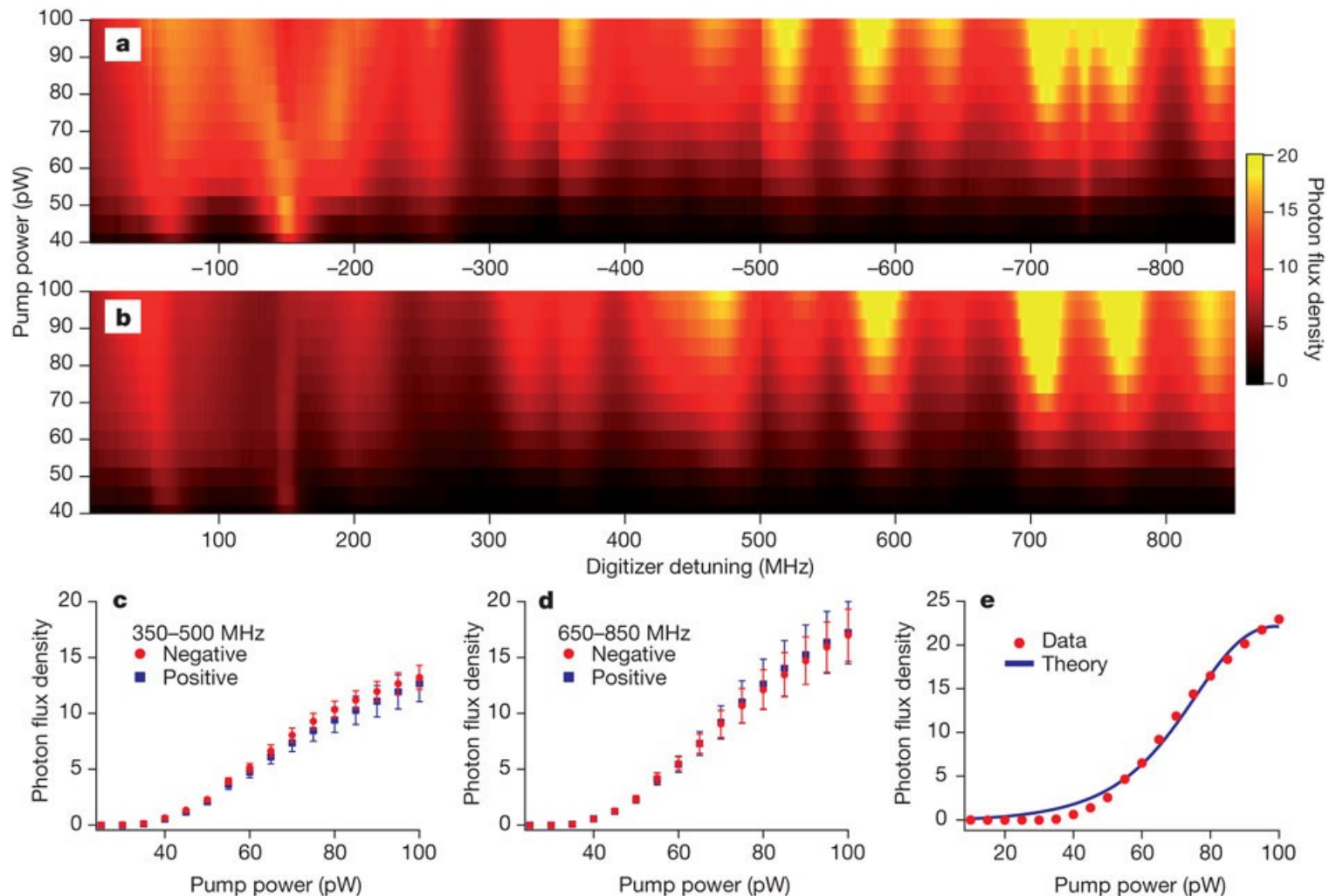
Fix the pump frequency and vary the analysis frequency:

We expect to see a symmetric spectrum around zero detuning from half the pump frequency.



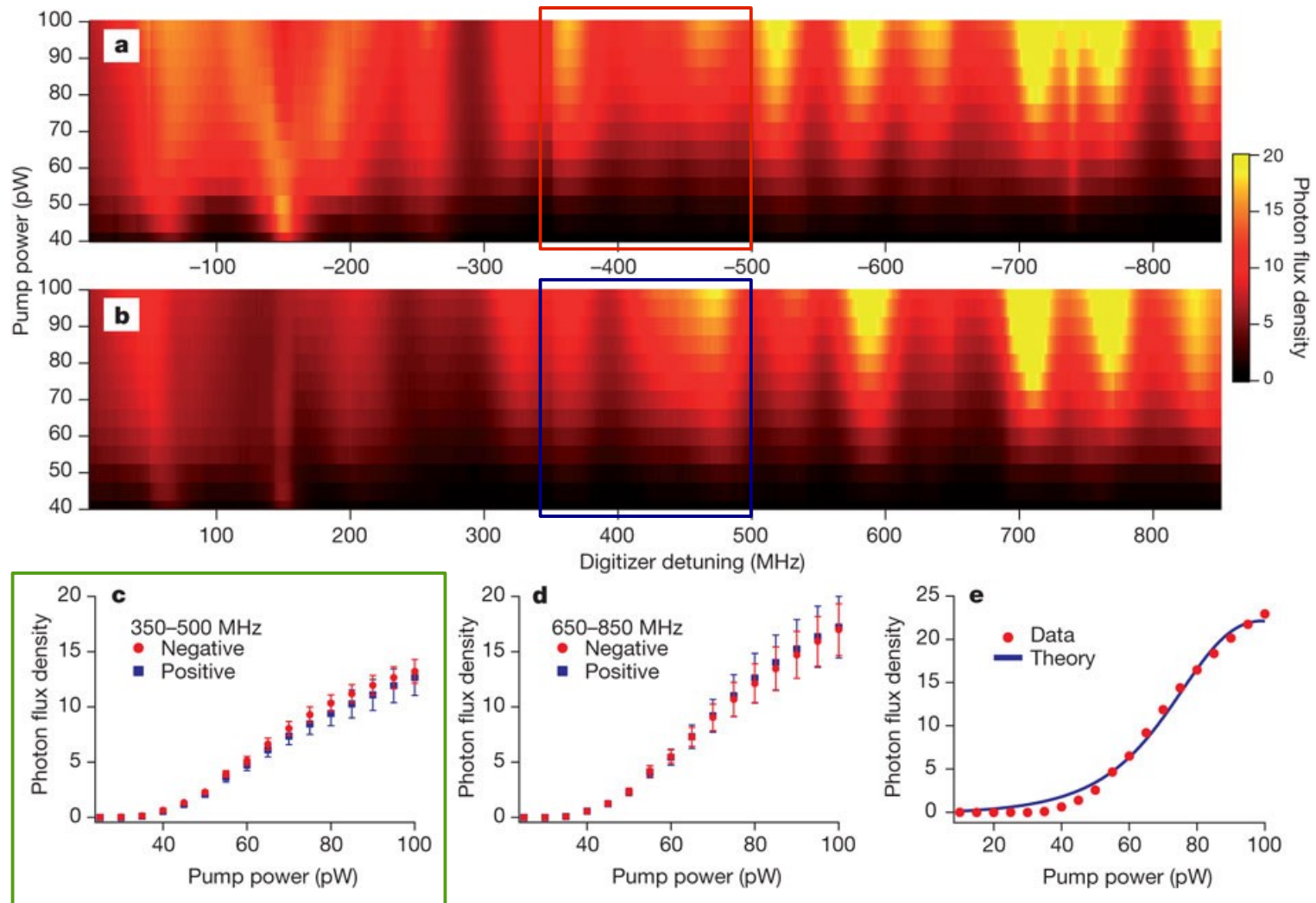
Measured photon-flux density: II

Broadband photon production is observed, and the measured spectrum is clearly symmetric around the half the pump frequency (zero digitizer detuning in figure below).



Measured photon-flux density: II

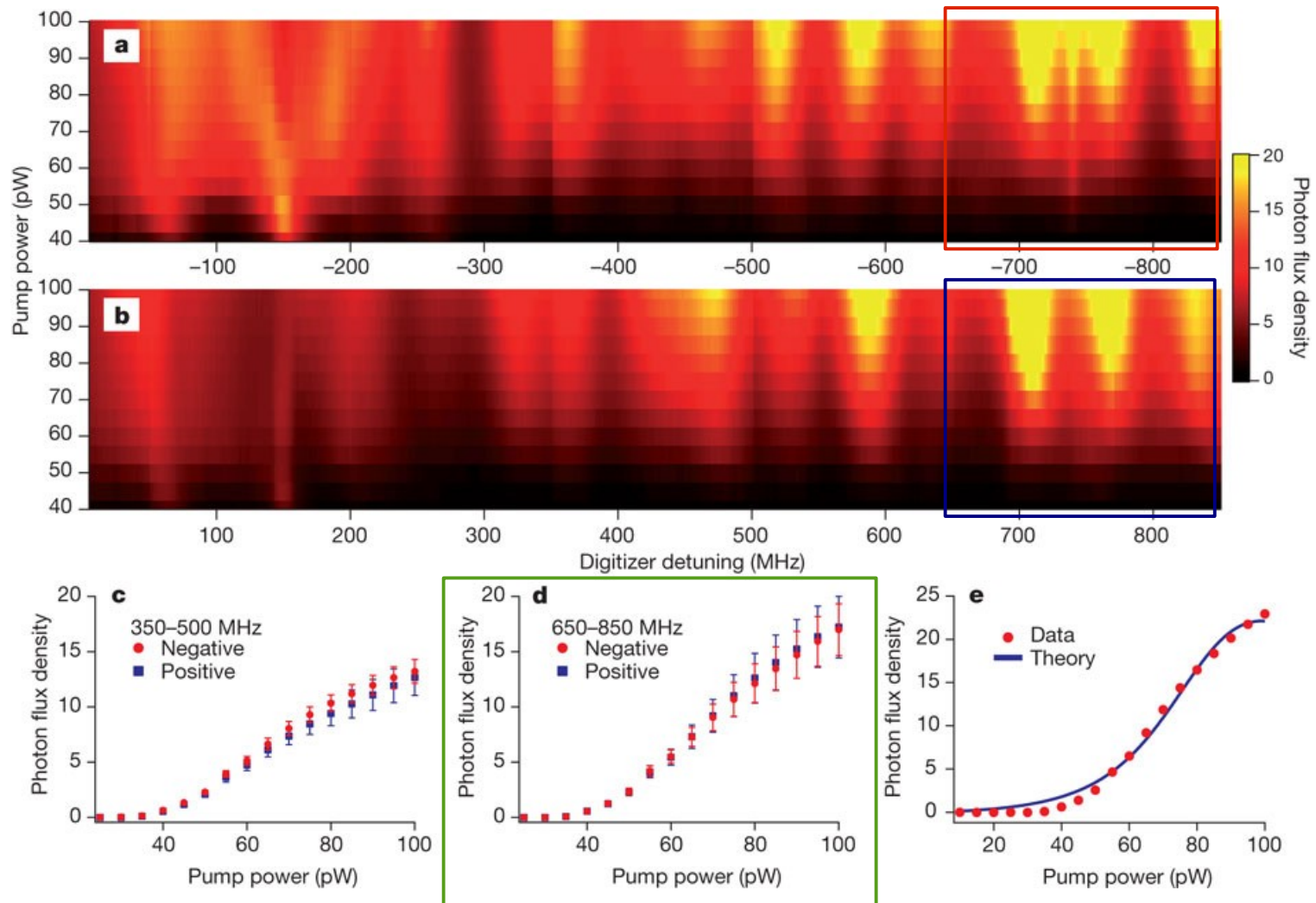
Broadband photon production is observed, and the measured spectrum is clearly symmetric around the half the pump frequency (zero digitizer detuning in figure below).



Averaged photon flux in the ranges indicated above

Measured photon-flux density: II

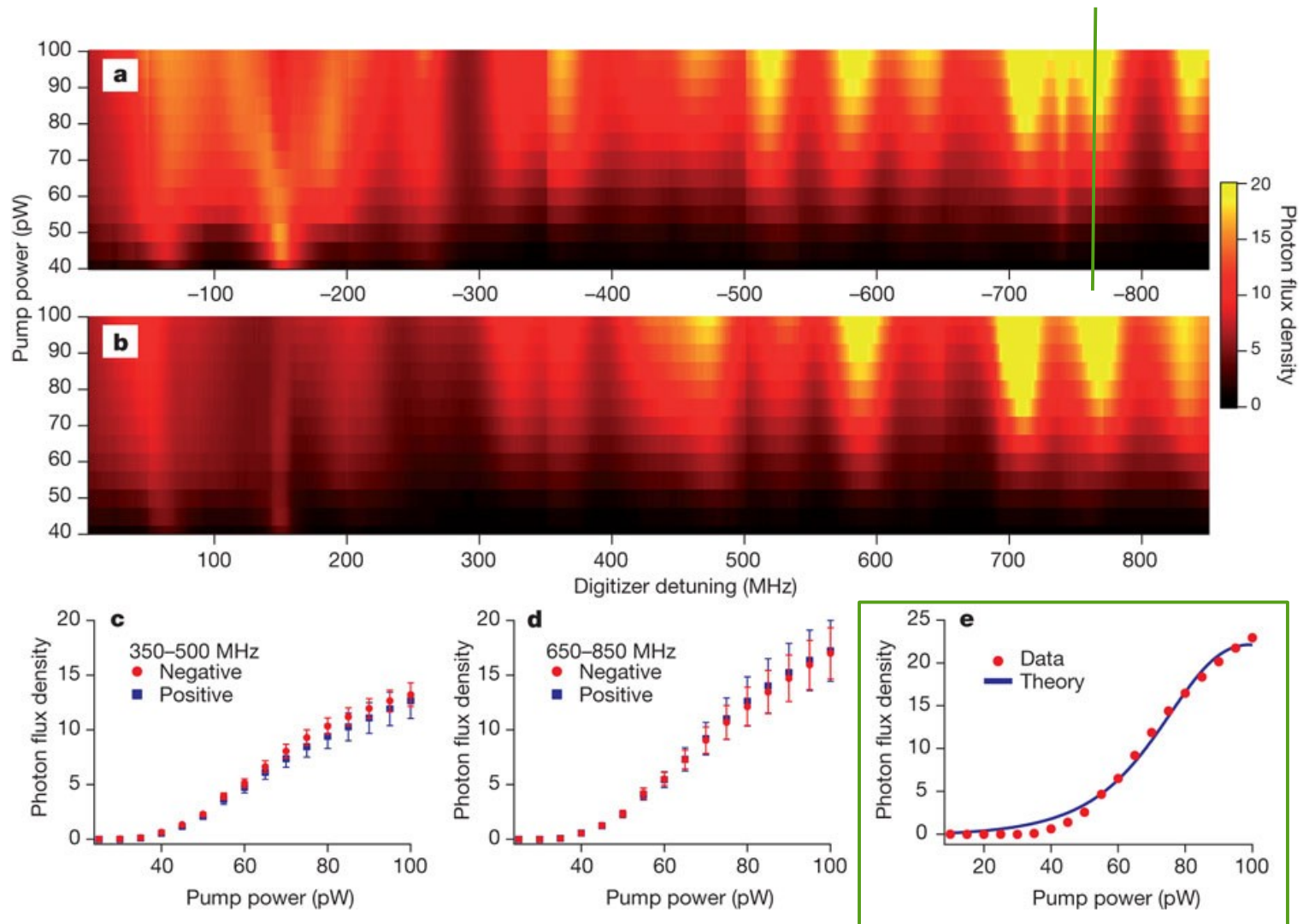
Broadband photon production is observed, and the measured spectrum is clearly symmetric around the half the pump frequency (zero digitizer detuning in figure below).



Averaged photon flux in the ranges indicated above

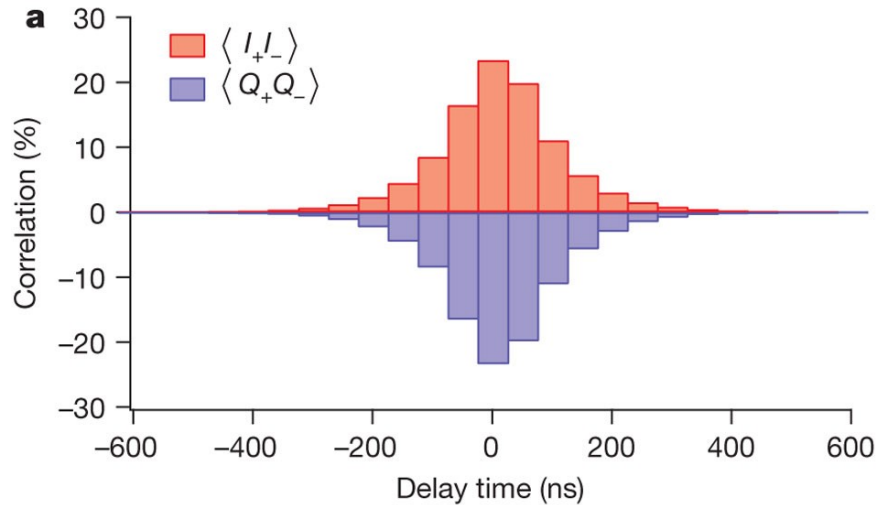
Measured photon-flux density: II

Broadband photon production is observed, and the measured spectrum is clearly symmetric around the half the pump frequency (zero digitizer detuning in figure below).



Photon flux vs pump power for the cut indicated above

Measured two-mode correlations and squeezing



Voltage quadratures:

$$I_{\pm} = \sqrt{\frac{\hbar\omega_{\pm}Z_0}{8\pi}} [a_{\text{out}}(\omega_{\pm}) + a_{\text{out}}(\omega_{\pm})^{\dagger}]$$

$$Q_{\pm} = -i\sqrt{\frac{\hbar\omega_{\pm}Z_0}{8\pi}} [a_{\text{out}}(\omega_{\pm}) - a_{\text{out}}(\omega_{\pm})^{\dagger}]$$

Symmetric around half the driving frequency:

$$\omega_{\pm} = \omega_d/2 \pm \delta\omega \quad \Rightarrow \quad \omega_+ + \omega_- = \omega_d$$

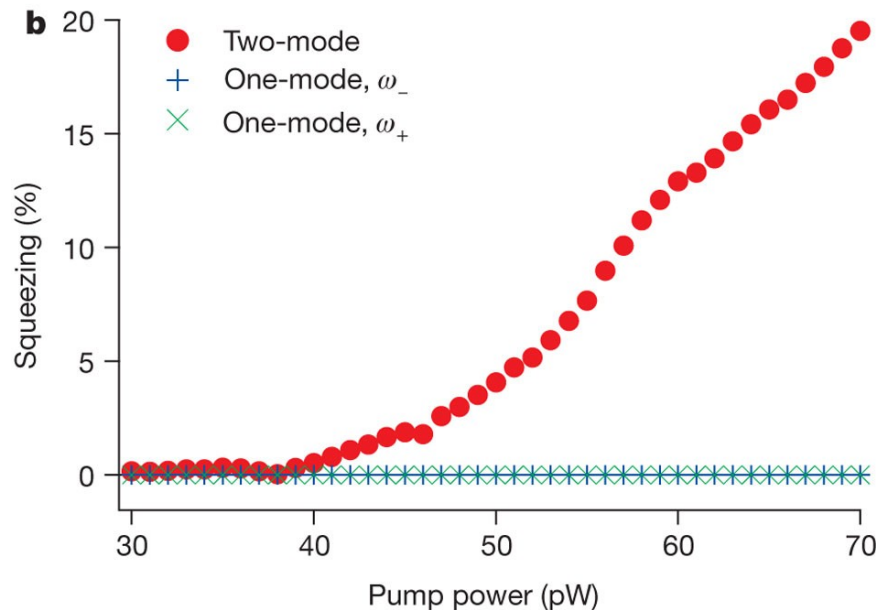
Strong two mode squeezing is observed (only) if

$$\omega_+ + \omega_- = \omega_d$$

→ strong indicator for photon-pair production.

Also, single-mode squeezing is not observed, as expected from the dynamical Casimir effect theory (where only two-photon correlations are created).

$$\sigma_2 = (\langle I_+ I_- \rangle - \langle Q_+ Q_- \rangle) / P_{\text{avg}}$$



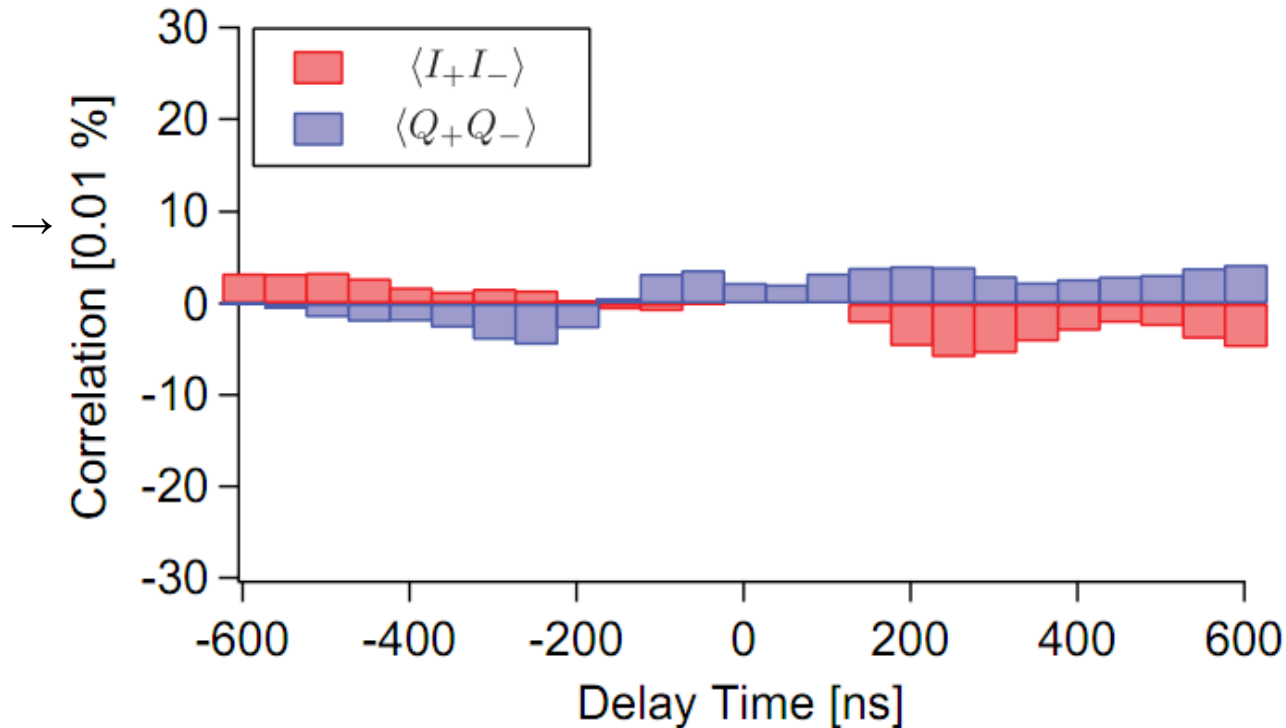
No correlations without pump signal

The correlations vanish when:

- the pump is turned off
- the two analysis frequencies does not sum up to the pump frequency:

$$\omega_+ + \omega_- \neq \omega_d$$

Compare to ~25% squeezing in the figure on the Previous page.



The parasitic cross-correlations intrinsic to the amplifier are very small.

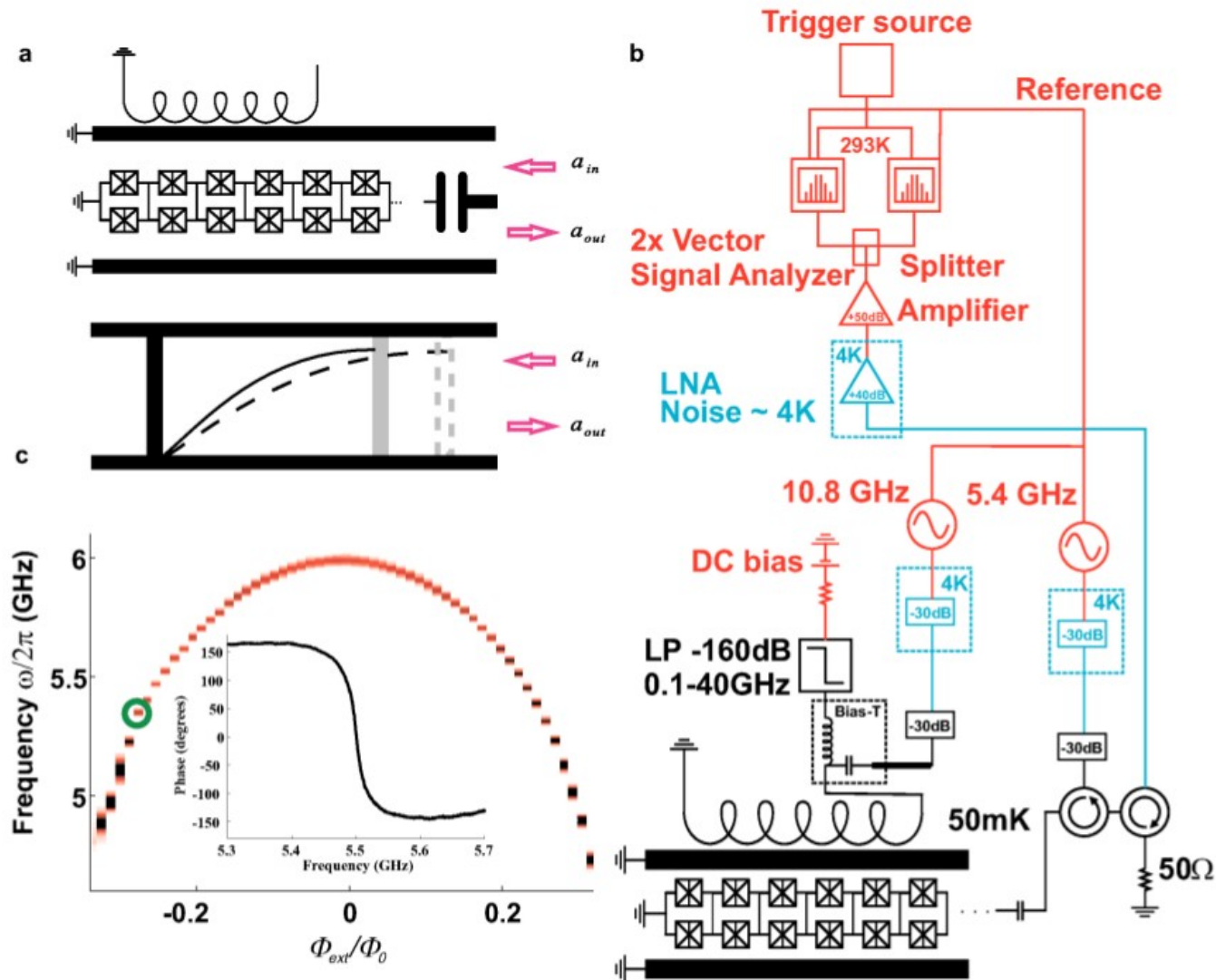
Experimental results

Wilson et al. Nature 2011

Lähteenmäki et al., PNAS (2013)

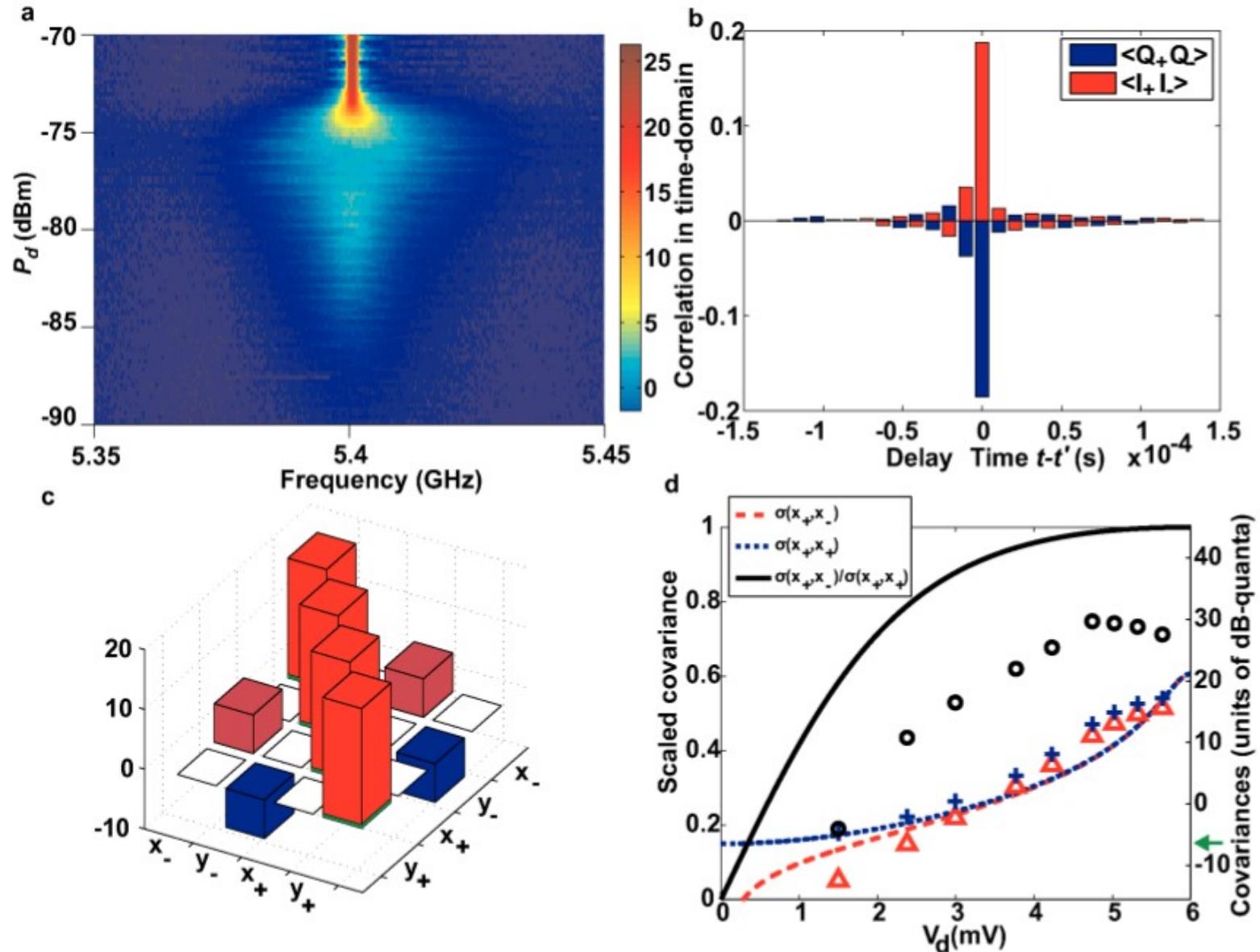
Experimental setup

Lähteenmäki et al., PNAS (2013)



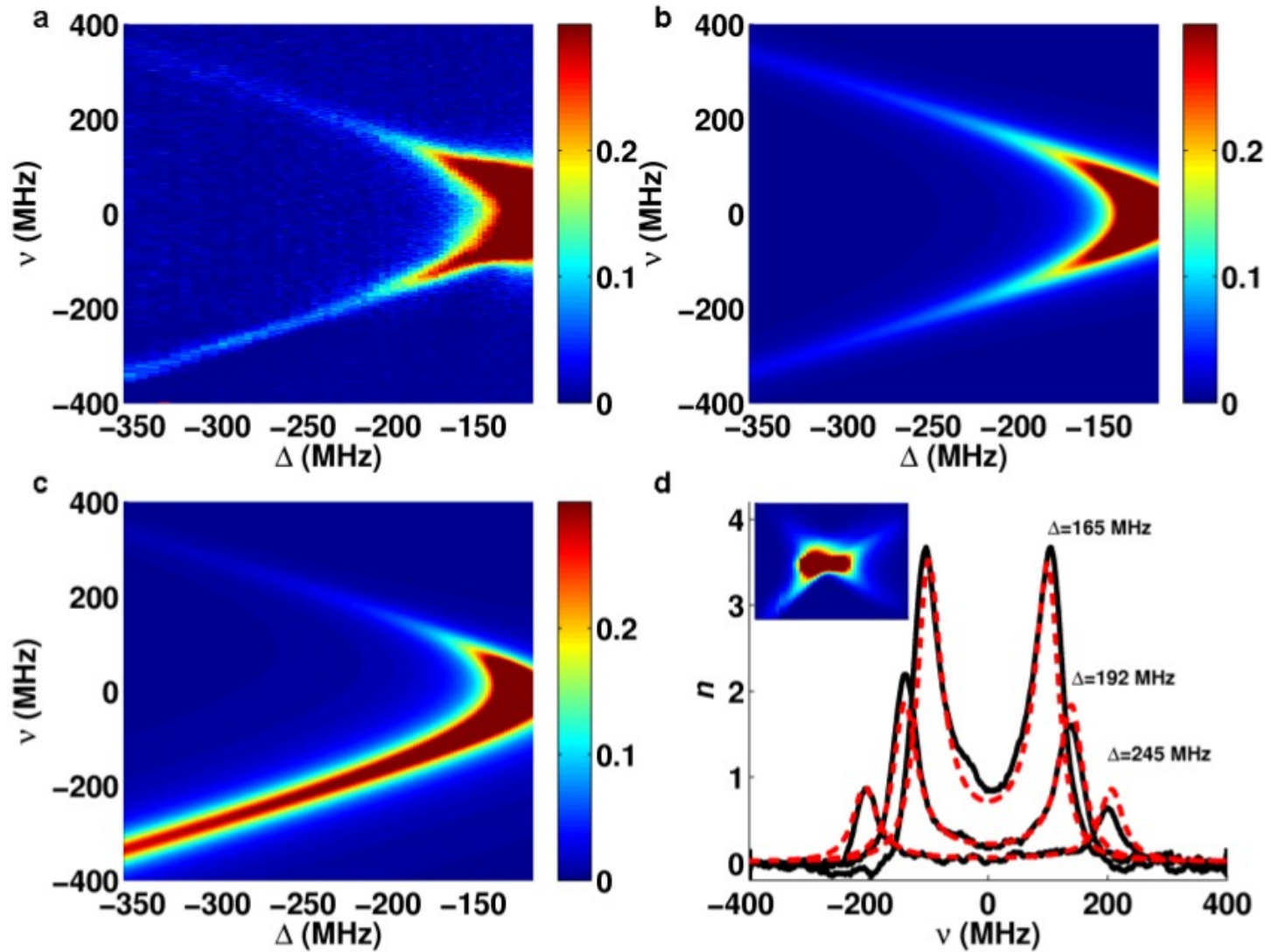
Measurements: two-mode correlations

Lähtenmäki et al., PNAS (2013)



Measurements: photon flux

Lähteenmäki et al., PNAS (2013)



More theory: nonclassicality tests

PRA 2013

Theory: Quantum-classical indicators

- Two-photon correlations and two-mode squeezing are nonclassical, but what about the entire field state including of thermal noise?

- Use a **nonclassicality test** based on the Glauber-Sudarshan P-function:

$$\langle : \hat{f}^\dagger \hat{f} : \rangle < 0 \rightarrow \text{nonclassical} \quad (\text{See e.g. Miranowicz PRA 2010})$$

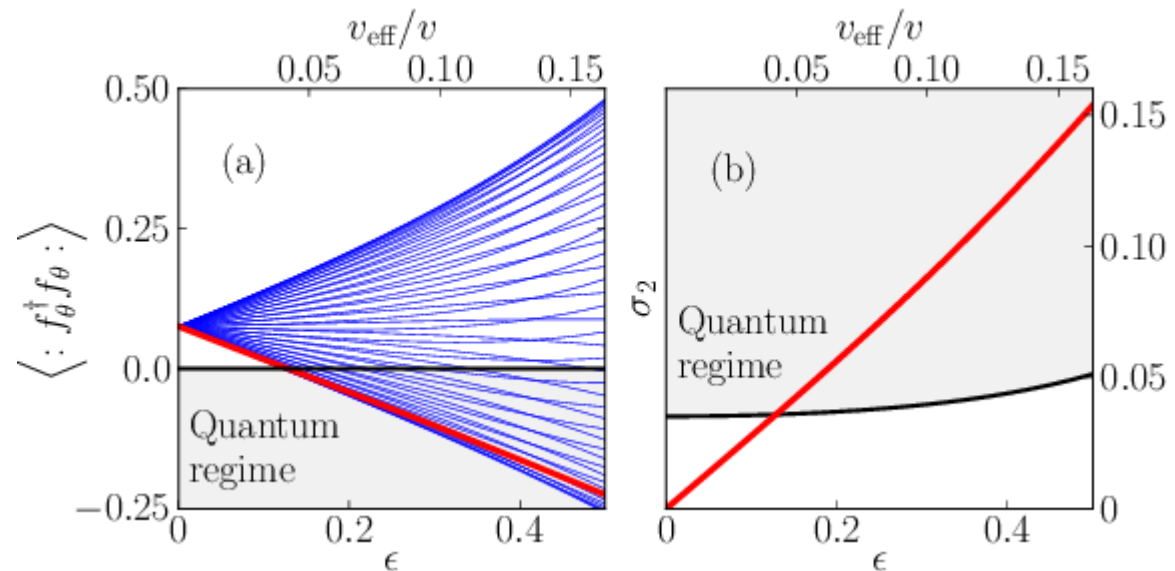
- For DCE in our circuit:

$$\hat{f}_\theta = e^{i\theta} \hat{b}_- + e^{-i\theta} \hat{b}_-^\dagger + i(e^{i\theta} \hat{b}_+ - e^{-i\theta} \hat{b}_+^\dagger) \quad (\text{good for cross-quadrature squeezing})$$

$$\langle : f_\theta^\dagger f_\theta : \rangle = 2(n_+^{\text{th}} + n_-^{\text{th}}) - 4 \cos 2\theta \frac{\delta L_{\text{eff}}}{v} \sqrt{\omega_+ \omega_-} (1 + n_+^{\text{th}} + n_-^{\text{th}})$$

$$\sigma_2 = \frac{(\langle I_+ I_- \rangle - \langle Q_+ Q_- \rangle)}{P_{\text{avg}}}$$

$$\epsilon = \frac{\delta L_{\text{eff}}}{v} \sqrt{\omega_+ \omega_-}$$



Theory: Quantum-classical indicators

- Alternative measure:

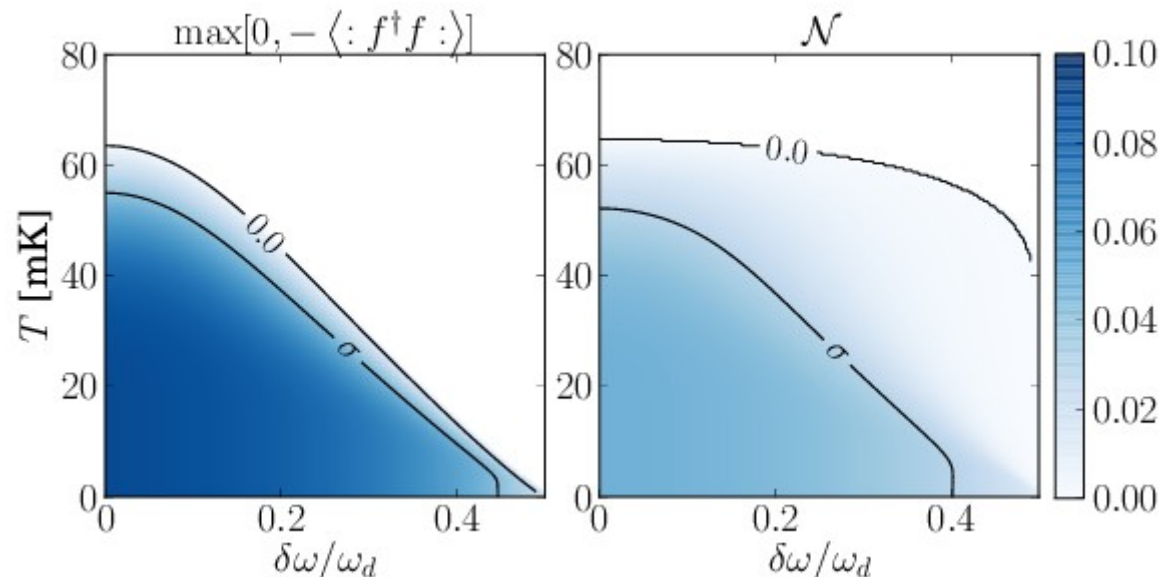
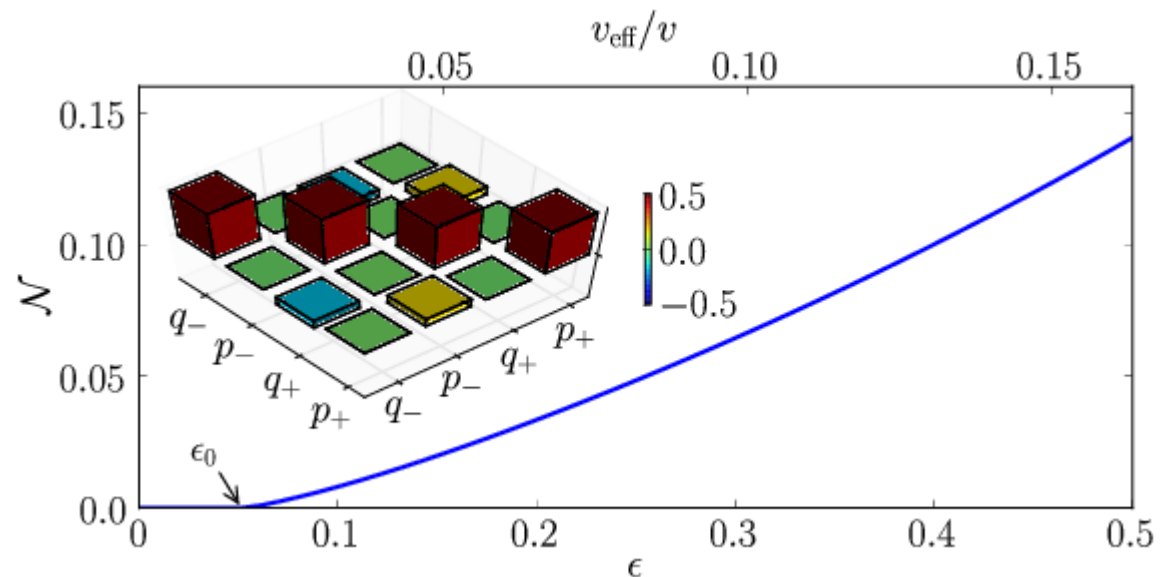
logarithmic negativity \mathcal{N}

- Stronger indicator than

$$\langle : \hat{f}^\dagger \hat{f} : \rangle < 0$$

but has the additional caveat that it is only valid for Gaussian states.

- Calculations with realistic circuit parameters suggests that both $\langle : \hat{f}^\dagger \hat{f} : \rangle$ and the logarithmic negativity indicates strictly nonclassical field states for the DCE radiation in a superconducting circuit.

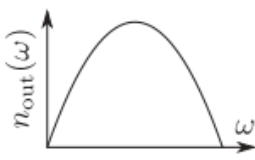
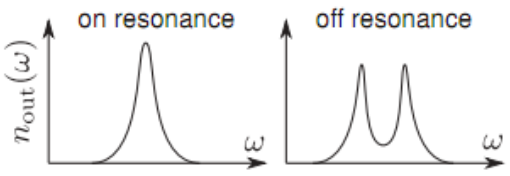



Conclusions

- Overview of superconducting circuits and quantum vacuum effects
- Introduced a circuit for the dynamical Casimir effect (DCE) in a superconducting coplanar waveguide (CPW):
 - Terminating the CPW with a SQUID allows the boundary condition to be tuned
 - We showed that this tunable boundary condition is equivalent to that of a perfect mirror at an effective distance that can be associated with the SQUID
 - That sinusoidally modulating the SQUID (effective length) results in broadband dynamical Casimir radiation consisting of two-mode correlated photons.
- Showed experimental measurements of:
 - The predicted broadband radiation
 - The expected two-mode correlations and symmetries.
 - Experimental demonstration of the dynamical Casimir effect.

Comparison between DCE w and w/o resonator

DCE in open waveguide, DCE in resonator and parametric oscillations/amplification (PO)

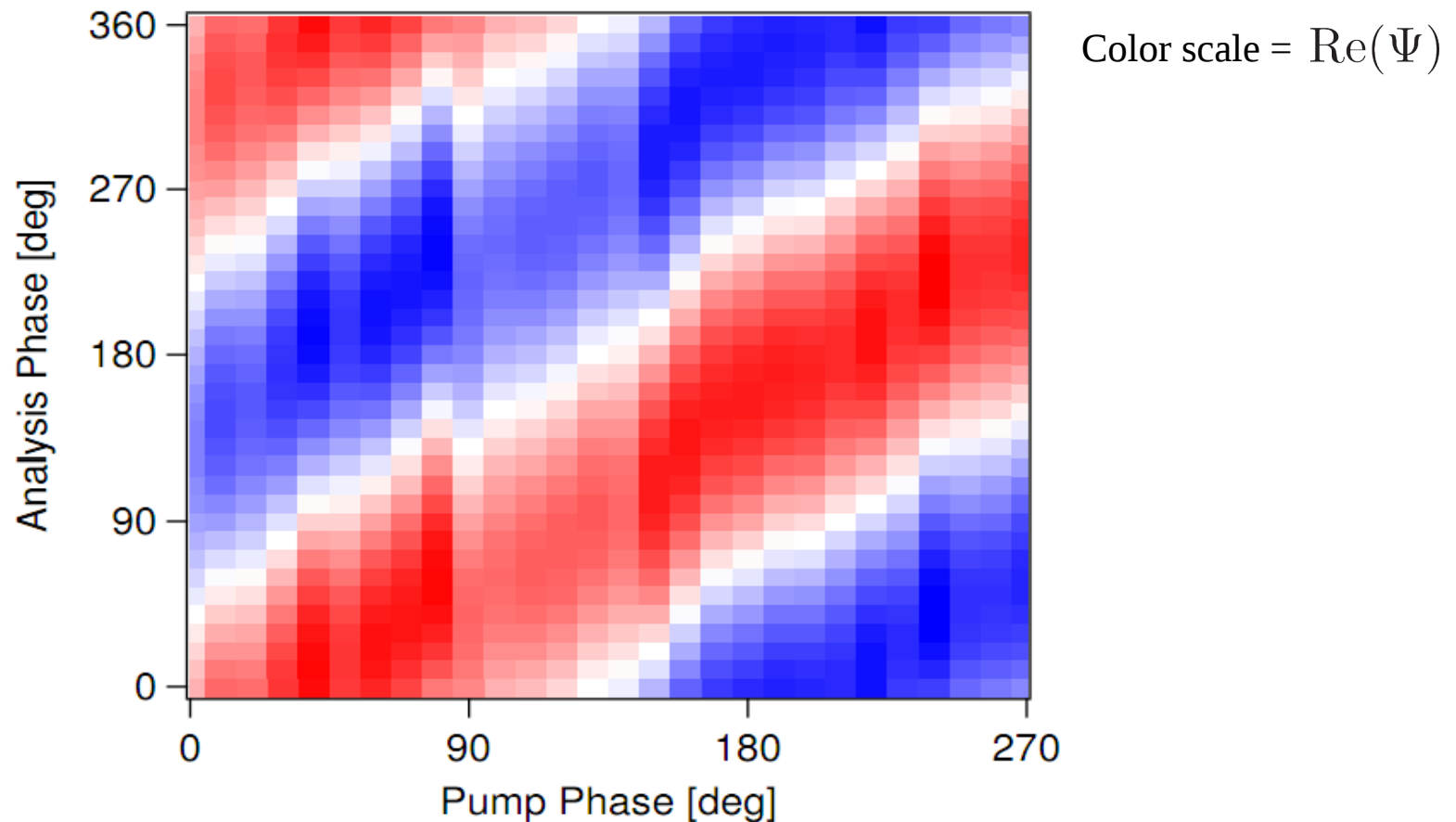
	Single-mirror DCE	Low- Q resonator DCE	High- Q resonator DCE/PO
Comments	Photons created due to time-dependent boundary condition	The resonator slightly alters the mode density, compared to the single-mirror case	DCE in a high- Q resonator is equivalent to a PO below threshold
Classical analog?	No, requires vacuum fluctuations	No, requires vacuum fluctuations	Yes, vacuum and thermal fluctuations give similar results
Resonance condition	No resonator	$\omega_{\text{res}} = \omega_d/2$	$\omega_{\text{res}} = \omega_d/2$
Threshold condition		$\epsilon_{\text{res}} \sim Q^{-1}$	$\epsilon_{\text{res}} \sim Q^{-1} \ll 1$ Above threshold, nonlinearity dominates behavior
Number of DCE photons per second	$\sim n(\omega_d/2)\omega_d$	$\sim n(\omega_{\text{res}})\Gamma$	$\sim n(\omega_{\text{res}})\Gamma$
Spectrum at $T = 0$ K	 <p>Broadband spectrum with peak at $\omega_d/2$</p>	 <p>Broad peaks at resonance frequency ω_{res} and the complementary frequency $\omega_d - \omega_{\text{res}}$</p>	 <p>Sharply peaked around the resonance frequency $\omega_{\text{res}} = \omega_d/2$</p>

Symmetry between pump and analysis phase

We also observe the symmetry between the pump and analysis phase of the correlator

$$\Psi = (\langle I_+ I_- \rangle - \langle Q_+ Q_- \rangle) + i (\langle I_+ Q_- \rangle + \langle I_- Q_+ \rangle)$$

that is expected for two-mode squeezed states.



Recent experimental results

Acoustic Analog to the Dynamical Casimir Effect in a Bose-Einstein Condensate

J.-C. Jaskula,^{*} G. B. Partridge,[†] M. Bonneau, R. Lopes, J. Ruaudel, D. Boiron, and C. I. Westbrook

Laboratoire Charles Fabry, Institut d'Optique, CNRS, Université Paris-Sud, 2 avenue Augustin Fresnel, 91127 Palaiseau, France

(Received 5 July 2012; published 26 November 2012)

We have modulated the density of a trapped Bose-Einstein condensate by changing the trap stiffness, thereby modulating the speed of sound. We observe the creation of correlated excitations with equal and opposite momenta, and show that for a well-defined modulation frequency, the frequency of the excitations is half that of the trap modulation frequency.

